A&A 578, A115 (2015)
DOI: 10.1051/0004-6361/201526270

Astronomy & Astrophysics

Herschel⋆ observations of extreme OH/IR stars

The isotopic ratios of oxygen as a sign-post for the stellar mass⋆⋆

K. Justtanont[1], M. J. Barlow[2], J. Blommaert[3,4], L. Decin[5], F. Kerschbaum[6], M. Matsuura[2,7], H. Olofsson[1], P. Owen[2], P. Royer[5], B. Swinyard[2,8,†], D. Teyssier[9], L. B. F. M. Waters[10,11], and J. Yates[2]

[1] Chalmers University of Technology, Onsala Space Observatory, 439 92 Onsala, Sweden
e-mail: kay.justtanont@chalmers.se
[2] University College London, Dept. of Physics & Astronomy, Gower Street, London, WC1E 6BT, UK
[3] Astronomy and Astrophysics Research Group, Dep. of Physics and Astrophysics, V.U. Brussel, Pleinlaan 2, 1050 Brussels, Belgium
[4] Flemish Institute of Technical Research, VITO, 2400 Mol, Belgium
[5] Instituut voor Sterrenkunde, Katholieke Universiteit Leuven, Celestijnenlaan 200D, 3001 Leuven, Belgium
[6] University of Vienna, Department of Astrophysics, Türkenschanzstrasse 17, 1180 Wien, Austria
[7] School of Physics and Astronomy, Cardiff University, Queen's Buildings, The Parade, Cardiff, CF24 3AA, UK
[8] Space Science and Technology Department, Rutherford Appleton Laboratory, Oxfordshire OX11 0QX, UK
[9] European Space Astronomy Centre, ESA, PO Box 78, 28691 Villanueva de la Cañada, Madrid, Spain
[10] SRON Netherlands Institute for Space Research, Sorbonnelaan 2, 3584 CA Utrecht, The Netherlands
[11] Sterrenkundig Instituut Anton Pannekoek, Universiteit van Amsterdam, Postbus 94249, 1090 GE Amsterdam, The Netherlands

Received 7 April 2015 / Accepted 11 May 2015

ABSTRACT

Aims. The late stages of stellar evolution are mainly governed by the mass of the stars. Low- and intermediate-mass stars lose copious amounts of mass during the asymptotic giant branch (AGB) which obscure the central star making it difficult to study the stellar spectra and determine the stellar mass. In this study, we present observational data that can be used to determine lower limits to the stellar mass.
Methods. Spectra of nine heavily reddened AGB stars taken by the *Herschel* Space Observatory display numerous molecular emission lines. The strongest emission lines are due to H_2O. We search for the presence of isotopologues of H_2O in these objects.
Results. We detected the ^{16}O and ^{17}O isotopologues of water in these stars, but lines due to $H_2^{18}O$ are absent. The lack of ^{18}O is predicted by a scenario where the star has undergone hot-bottom burning which preferentially destroys ^{18}O relative to ^{16}O and ^{17}O. From stellar evolution calculations, this process is thought to occur when the stellar mass is above 5 $M_\odot$ for solar metallicity. Hence, observations of different isotopologues of H_2O can be used to help determine the lower limit to the initial stellar mass.
Conclusions. From our observations, we deduce that these extreme OH/IR stars are intermediate-mass stars with masses of ≥5 $M_\odot$. Their high mass-loss rates of $\sim 10^{-4}$ $M_\odot$ yr^{-1} may affect the enrichment of the interstellar medium and the overall chemical evolution of our Galaxy.

Key words. stars: AGB and post-AGB – stars: mass-loss – circumstellar matter – stars: evolution – submillimeter: stars

1. Introduction

Low- and intermediate-mass stars (0.8−8 $M_\odot$) evolve onto the asymptotic giant branch (AGB) after exhaustion of the central He. During this phase, the stars continue nucleosynthesis in a thin shell of He, surrounded by a larger H-burning shell (e.g., Iben & Renzini 1983; Habing 1996). During its AGB lifetime, a star experiences a number of He-flashes that lead to a sudden increase in its luminosity over a brief period of time. Owing to efficient convection inside the star, the nucleosynthesis products are mixed outwards (the so-called third dredge-up). Fresh carbon produced in the He-shell burning is transported to the stellar photosphere and will increase the carbon-to-oxygen ratio, which can turn the originally oxygen-rich stars into carbon-rich stars.

The exact outcome of the nucleosynthesis and mixing events on the stellar surface abundance depends on the stellar mass. This is especially true when it comes to the process called hot-bottom burning, where the base of the convective zone of the hydrogen envelope is hot enough for CNO-cycle burning to destroy carbon (Lattanzio & Wood 2003). There is observational evidence that the process of hot-bottom burning occurs. Sackmann & Boothroyd (1992) observed a number of stars that exhibit anomalously high lithium abundance which is thought to be a byproduct of hot-bottom burning. This process is also thought to prevent a star from becoming carbon-rich. The minimum limit of the stellar mass that can trigger this process is estimated to be ≥5 $M_\odot$ for stars with a solar metallicity and can be smaller for lower metallicities (Karakas & Lattanzio 2014). Another signpost that AGB stars are descendants of such intermediate-mass main-sequence stars is a low $^{12}C/^{13}C$ ratio – during the AGB phase, more massive intermediate-mass stars enter the CNO cycle which tends to produce ^{13}C while converting ^{12}C to ^{14}N. The presence of ^{13}C is the main neutron source for the s-process elements (Busso et al. 1999; Herwig 2005).

⋆ *Herschel* is an ESA space observatory with science instruments provided by European-led Principal Investigator consortia and with important participation from NASA.
⋆⋆ Tables 3, 4 and Appendices are available in electronic form at http://www.aanda.org
† Bruce Swinyard passed away on 22/5/2015 after a long fight with cancer. His contribution to this work is very much appreciated.

Another possible route is thought to be from the ^{22}Ne source in intermediate-mass stars, which requires a higher temperature.

An attempt to estimate masses of OH/IR stars near the galactic centre was carried out by Wood et al. (1998). They derived a mass of ~4 $M_\odot$ for many of the stars in the sample using a period-luminosity relationship. Two stars with the longest periods were thought to have masses of up to 7 $M_\odot$. A number of optically visible OH/IR stars have been observed to exhibit a high Li abundance but show weak s-process elements (García-Hernández et al. 2007, 2013). These authors conclude that the stars have undergone hot-bottom burning but that there is a mechanism that delays the onset of s-process element production (Karakas et al. 2012). For OH/IR stars with an optically thick circumstellar envelope, which prevents the direct determination of stellar abundance, other hot-bottom burning indicators must be used. Two such stars (AFGL 5379 and OH 26.5+0.6) have been observed with the *Herschel* Space Observatory (hereafter *Herschel*, Pilbratt et al. 2010) to have strong water emission lines in $H_2^{16}O$ and $H_2^{17}O$ but no detection of the $H_2^{18}O$ line (Justtanont et al. 2013). An AGB evolutionary model for a 5 $M_\odot$ star by Lattanzio & Wood (2003) shows that during hot-bottom burning, ^{18}O is preferentially destroyed with respect to the other two isotopes. The *Herschel* observations of ^{18}O/^{17}O ratios of $\ll$1 for these two stars are in contrast to the value of ~3 derived from the interstellar medium (Wilson & Rood 1994).

In this paper, we present a larger sample of extreme OH/IR stars – those with very dusty circumstellar envelopes such that silicate dust features at 10 and 20 μm are in absorption, indicating high ($\dot{M} \geq 10^{-4}$ $M_\odot$ yr^{-1}) mass-loss rates. The observations of these stars were taken with all three instruments on board *Herschel* in order to search for the emission lines of three isotopologues of H_2O as signposts for hot-bottom burning, with the aim to obtain a lower limit to the stellar mass. Detailed modelling of the line emission of H_2O and other detected molecules will be presented in the future papers. In Sect. 2, we present the *Herschel* observations obtained as part of an open-time program on OH/IR stars. We discuss the results of our observations in Sect. 3 and summarize our findings in Sect. 4.

2. Observations

We obtained *Herschel* spectra of eight OH/IR stars selected from the sample based on Justtanont et al. (2006). These stars all exhibit the silicate dust features in absorption at both 10 and 18 μm and in some cases also show a water-ice band at 3.1 μm. Table 1 lists all stars observed and presented in this paper for the first time using the three *Herschel* instruments PACS, HIFI, and SPIRE. As noted, some stars have had their spectra taken as part of either a guaranteed time or another open-time program.

We observed four extreme OH/IR stars with the *Herschel*-HIFI instrument (de Graauw et al. 2010), which happened to be the last set of observations that *Herschel* did before the helium ran out at the end of April 2013 (Fig. 1). The frequency coverage for these stars are 1094.3−1098.4 GHz (lower side-band, LSB) and 1106.3−1110.4 GHz (upper side-band, USB). The LSB frequency covers the ortho-H_2O transition of 3_{12}−3_{03} for all three isotopologues while the USB permits the observations of the ground state transition of para-$H_2^{17}O$ 1_{11}−0_{00}. The raw data (level 0) were processed with pipeline version SPG 11.0 to obtain the level 1 and 2 data. Further data reduction was performed in HIPE12[1] (Ott 2010) with calibration files version HIFI_CAL_15. Both polarizations were averaged together and the final spectra had the baseline subtracted and rebinned. From Fig. 1 it can bee seen that all objects, with the exception of OH 30.7+0.4, show the emission line due to $H_2^{16}O$. Using a routine in HIPE12, we converted the antenna temperature to a flux scale so that we have the same flux scale for all three instruments, assuming a point source. The line fluxes are listed in Table 2.

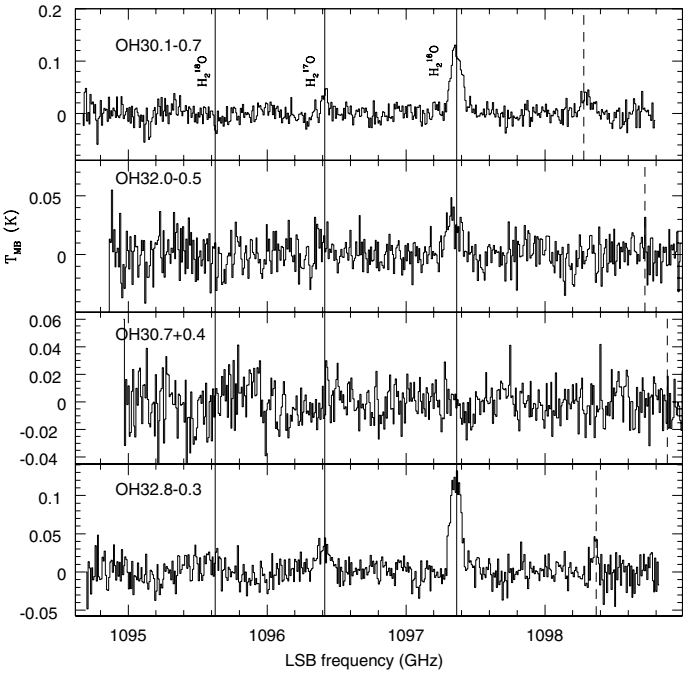

Fig. 1. *Herschel*-HIFI observation of four extreme OH/IR stars. The spectra have been corrected for the LSR velocity for each object and rebinned to ~2 km s^{-1} sampling. The vertical lines indicate the expected position of the $H_2^{18}O$, $H_2^{17}O$, and $H_2^{16}O$ 3_{12}−3_{03} transitions, from left to right. The expected position of the $H_2^{17}O$ 1_{11}−0_{00} transition (dashed line) from the upper side-band can be seen at the far right.

We obtained SPIRE spectra of eight extreme OH/IR stars and included OH 26.5+0.6 from the archive. The resolution of these spectra is ~1.4 GHz, corresponding to 380 km s^{-1} at a frequency of 1097 GHz hence the lines are not resolved and each observed emission line can be a blend of different molecules. With the help of the HIFI spectra of OH/IR stars (Justtanont et al. 2012), we can resolve the contribution of strong emission lines mainly due to H_2O and CO.

The SPIRE data were reduced using the calibration files SPIRE_CAL_12_2. The spectra suffer from high backgrounds due to the location of these objects in the galactic plane and most stars are thought to have a typical distance larger than 1 kpc. Interstellar emission lines due to [N II] at 205.178 μm and [C I] at 370.423 and 609.150 μm can be seen in the spectra, with the exception of AFGL 5379 which is thought to be closer than the other objects. We performed background subtraction from our spectra by investigating individual off-centre beams and selected those that have similar background levels as the central beam. However, the region between 300−400 μm is badly affected so that it is difficult to recover background subtracted data.

A number of the stars observed with SPIRE have been observed using the PACS instrument. Together with the PACS data taken by the MESS guaranteed time program (Groenewegen et al. 2011) for AFGL 5379 and from another open-time program (PI. M.J. Barlow) for OH 26.5+0.6, we have full spectral

[1] HCSS/HSpot/HIPE is are joint developments by the *Herschel* Science Ground Segment Consortium, consisting of ESA, the NASA *Herschel* Science Center, and the HIFI, PACS, and SPIRE consortia.

Table 1. OH/IR stars observed in the present work with observation identifiers (ObsID) indicated.

Source	RA (2000)	Dec (2000)	ObsIDs			Note
			SPIRE	PACS	HIFI	
OH 127.8+0.0	01 33 51.2	+62 26 53.2	1342268319	1342189956−1342189961	–	PACS cal
AFGL 5379	17 44 24.0	−31 55 35.5	1342268287	1342228537/1342228538	1342250605	1, 2
OH 21.5+0.5	18 28 31.6	−09 58 10.7	1342268311	1342268748/1342268778	–	
OH 26.5+0.6	18 37 32.5	−05 23 59.2	1342243624	1342207776/1342207777	1342244511	1, 2, 3
OH 30.7+0.4	18 45 53.1	−01 46 58	1342268309	1342268789/1342268790	1342271263	
OH 30.1-0.7	18 48 41.9	−02 50 28.3	1342268316	1342269304/1342269305	1342271264	
OH 32.0-0.5	18 51 26.2	−01 03 52	1342268317	1342268791/1342268792	1342271265	
OH 32.8-0.3	18 52 22.2	−00 14 13.9	1342268318	1342268793/1342268794	1342271266	
OH 42.3-0.1	19 09 07.5	+08 16 22.5	1342268308	1342268797/1342268798	–	

Notes. The archived data taken from guaranteed time programs are indicated as 1 from MESS, 2 from HIFISTARS and 3 from another open-time program. The PACS spectra of OH 127.8 were taken as part of the calibration time.

Table 2. Line fluxes of isotopologues of H_2O in the observed HIFI range.

$\lambda(\mu m)$	Transition	Isotope	Line fluxes ($\times 10^{-17}$ W m^{-2})				
			GL5379	OH26.5	OH30.1	OH32.0	OH32.8
269.272	$1_{11}-0_{00}$	16	18.2	8.3	a	a	a
270.774	$1_{11}-0_{00}$	17	9.2	3.6	1.1	0.6	1.0
272.118	$1_{11}-0_{00}$	18	<0.8	<0.6	a	a	a
273.193	$3_{12}-3_{03}$	16	29.7	11.0	4.9	2.0	4.7
273.430	$3_{12}-3_{03}$	17	9.1	3.8	1.0	0.8	1.9
273.626	$3_{12}-3_{03}$	18	<0.8	<0.6	<0.4	<0.3	<0.4

Notes. "a" indicates that the transition is not observed. The fluxes for $H_2^{18}O$ indicate the upper limit of the detection and as such can be regarded as an estimated uncertainty of the calculated line fluxes.

coverage from 50 to 670 μm for all the stars in our sample. For OH 127.8+0.0, the data were taken as part of the calibration time (Lombaert et al. 2013). We used the calibration files PACS_CAL_48_0 for our targets. The flux from the central 3×3 spaxels were extracted. We note that the data suffer from significant leakage in the red part of the spectrum, which means that the data between 95−100 μm and beyond ∼190 μm cannot be recovered.

In the PACS spectral range, we identify the emission lines as coming from H_2O, and CO plus three sets of lines due to OH at 79, 119, and 163 μm (Fig. 4 and Appendix C). These lines have previously been reported by Sylvester et al. (1997) and Lombaert et al. (2013) and are thought to be the pumping line for the OH masers seen in these objects. Although the archived spectra from the short-wavelength spectrometer (LWS, Clegg et al. 1996) aboard the Infrared Space Observatory (ISO, Kessler et al. 1996) of some of these stars are very noisy, there may be a possible hint of an absorption of the infrared pumping line at 53 μm. The other infrared pumping line at 34.6 μm was first reported towards two supergiants (Justtanont et al. 1996; Sylvester et al. 1997), but has not been detected towards AGB stars observed with ISO. No strong emission lines due to other molecules apart from H_2O, OH, and CO have been reported from OH 127.8+0.0 (Lombaert et al. 2013).

3. Discussion

Justtanont et al. (2013) found strong $H_2^{16}O$ and $H_2^{17}O$ emission lines in two extreme OH/IR stars, AFGL 5379 and OH 26.5+0.6, while there is no detectable emission due to $H_2^{18}O$. This is in contrast to what is observed in the interstellar medium and the Sun (Wilson & Rood 1994) where ^{18}O is more abundant than ^{17}O. The question arises if other extreme OH/IR stars show the same behaviour.

3.1. Resolved HIFI spectra

In four objects, we obtained HIFI spectra that cover the frequency range of the $3_{12}-3_{03}$ line for all three isotopologues. From Fig. 1, we detect the main line at 1097.365 GHz (273.200 μm) in all the sources except OH 30.7+0.4. The expansion velocity of these stars is typically 15 km s^{-1}, hence with an observed velocity resolution of 1 km s^1 the line is well resolved. The spectrum of OH 32.0-0.5 is too noisy to confirm the detection of $H_2^{17}O$ at 1096.414 GHz (273.430 μm); $H_2^{17}O$ can be seen in OH 30.1-0.7 and OH 32.8-0.3, along with the $H_2^{17}O$ $1_{11}-0_{00}$ line from the upper side-band. No evidence of the $H_2^{18}O$ $3_{12}-3_{03}$ line at 1095.627 GHz (273.626 μm) is seen in our spectra (Table 2). This is similar to the non-detection of $H_2^{18}O$ in AFGL 5379 and OH 26.5+0.6 where both $H_2^{16}O$ and $H_2^{17}O$ lines are clearly detected (Justtanont et al. 2013).

Based on these observations, we searched for the presence of all isotopologues of H_2O in the SPIRE and PACS spectra.

3.2. SPIRE spectra

In these spectra, we are able to discern a number of possible $H_2^{17}O$ lines. The SPIRE spectrum of AFGL 5379 (Figs. 2 and 3) shows the identification of both isotopologues, along with other molecules such as CO, SiO, HCN, and H_2S (see Appendix B) although the lines are not resolved owing to the poor spectral resolution of the SPIRE instrument ($\lambda/\Delta\lambda \sim 370-1290$ for

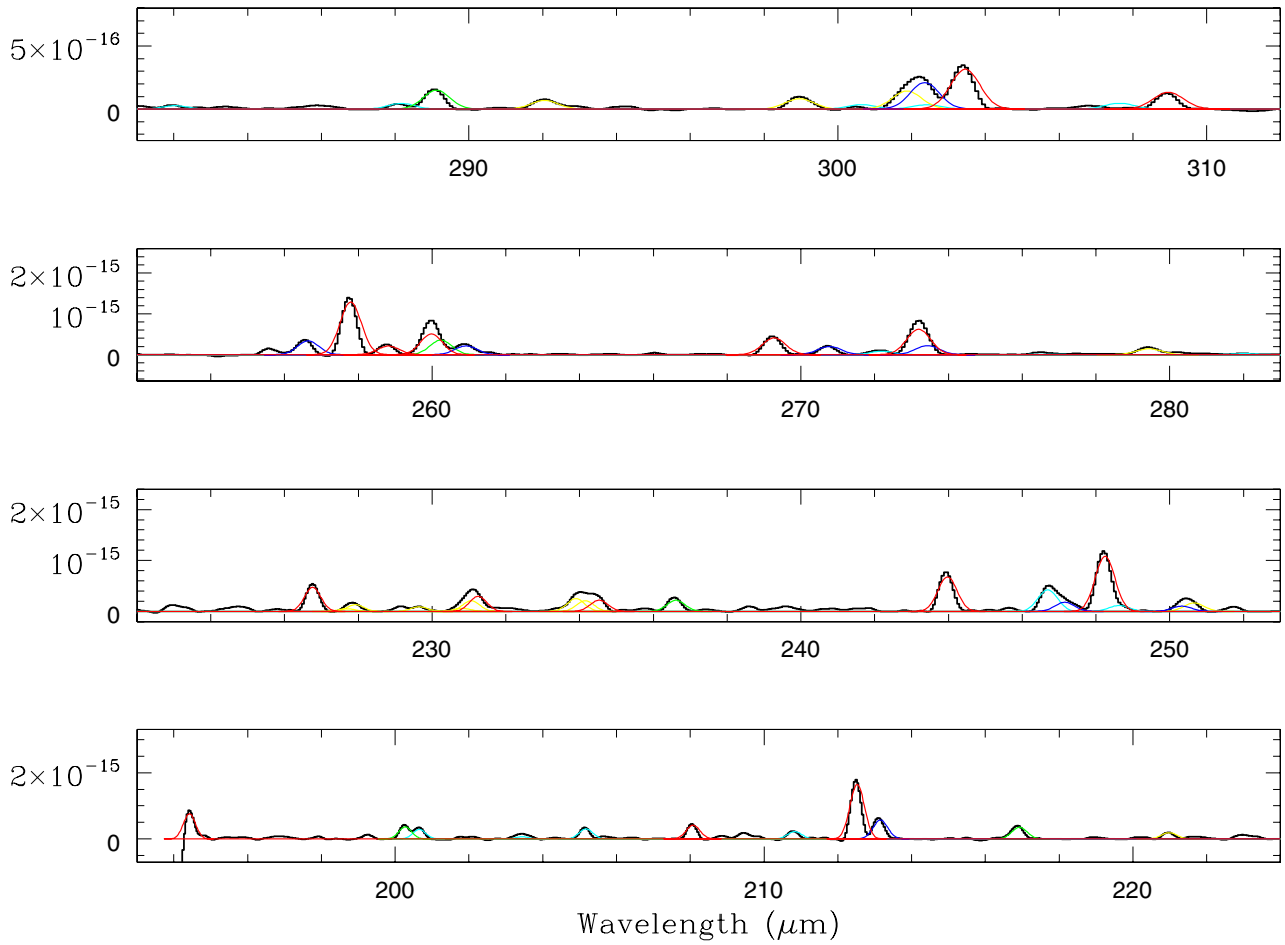

Fig. 2. The continuum subtracted apodized SPIRE spectrum of AFGL 5379 (histogram) with the Gaussian fits for H_2O (red), $H_2^{17}O$ (blue), CO (green), and H_2S (yellow). Other molecules such as SiO, HCN, and the interstellar lines of [C I] and [N II] are shown in cyan. The flux for SPIRE and PACS spectra is in W m^{-2} μm^{-1}.

670−194 μm). In order to calculate the line fluxes, we employed the special script in the HIPE data reduction package written for unapodized SPIRE data (SPIRE_linefitting.py), taking into account the fit to the sinc function of the line profiles. For display purposes, we show the apodized spectra (with the sinc function corrected) together with the calculated Gaussian line profiles because the lines are unresolved, with a width of 0.078 cm^{-1} for unapodized spectra, i.e. $F_{\rm line} = 1.08 \times F_{\rm peak} \times FWHM$. However, one caveat of the derived line fluxes is that the decomposed molecular components depend only on the central frequencies of the lines and not on the expected transition line strengths. For this purpose we include species thath exhibit several transitions and select lines within the SPIRE range with an upper energy ≤1000 K. We did, however, add an exception for the H_2O ν_2 transitions as these lines can sometimes be bright when they are masing. We listed the pair of detected $H_2^{16}O$ and $H_2^{17}O$ fluxes in Table 3. The estimated uncertainty for unblended lines is 30%, increasing to ∼50% for blended lines. For our purpose, blended lines are defined as lines that have two or more species that are separated by less than the spectral resolution of the instrument and so the peaks are indistinguishable. In many cases, there are lines that overlap with distinct peaks which makes the line flux determination cleaner than the blended lines. We note that a series of lines due to H_2S are detected in the SPIRE wavelength range for most of our objects. The full list of all the lines detected and plots of the SPIRE spectra observed can be found in Appendix B and D, respectively.

3.3. PACS spectra

For the PACS spectra, we fitted a Gaussian to individual lines to derive a line flux as the lines are also unresolved with a resolving power of 1000−5000, corresponding to a velocity resolution of ∼300−60 km s^{-1}, for the long and short wavelengths, respectively. Since most of the lines are due to H_2O, we decided to fit these before attributing the unfitted lines to other molecules such as CO and H_2S. Figure 4 shows the continuum subtracted spectrum of AFGL 5379. Unfortunately, the source was not at the central spaxel when it was observed. This resulted in a loss of flux. However, we corrected this based on the archived ISO-LWS continuum flux data. The PACS data have been multiplied by a factor of 1.78 to get the flux to agree with the ISO-LWS flux. Another artefact is that the shortest wavelength part of the PACS spectrum cannot be recovered as it is badly affected by the foreground and background interstellar [O I] 63 emission. We did not detect any emission lines in the PACS spectrum of OH 21.5+0.5. The PACS spectrum of OH 30.7+0.4 does not show definitive detections of $H_2^{17}O$ lines. These two objects are hence not listed in Table 4.

The line fluxes of $H_2^{16}O$ and $H_2^{17}O$ are listed in Table 4. The estimated uncertainty for each derived line flux depends on the errors in baseline subtraction and the rms noise of the spectrum which can affect the flux by ∼30%. Two $H_2^{17}O$ lines at 57.74 and 67.51 μm are close in wavelength to much higher excited lines of H_2O $8_{17}-7_{26}$ and $11_{48}-11_{39}$, with upper energy levels

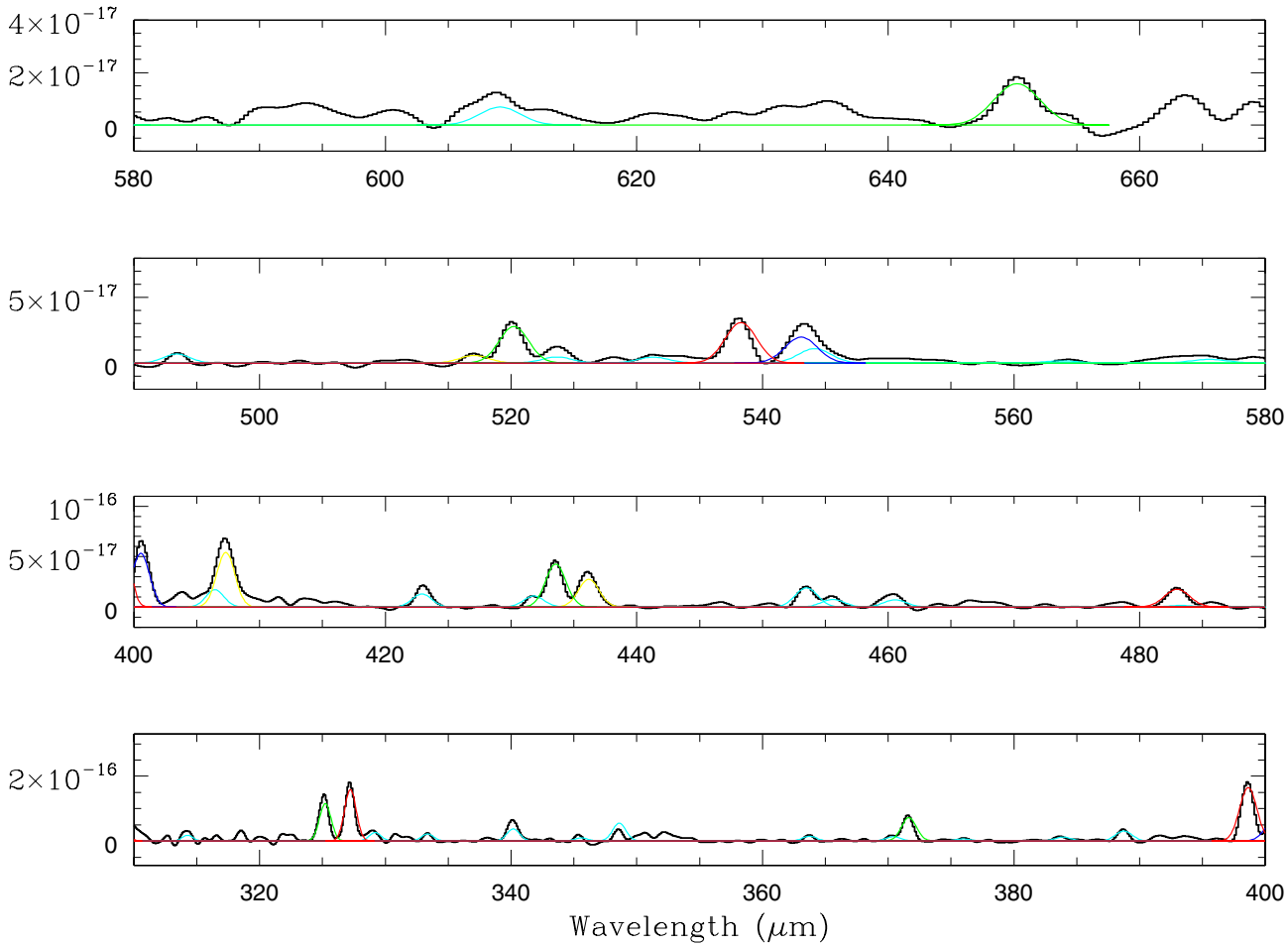

Fig. 3. The continuum subtracted apodized SPIRE spectrum of AFGL 5379 (histogram) with the Gaussian fits for H_2O (red), $H_2^{17}O$ (blue), CO (green), and H_2S (yellow). Other molecules are shown in cyan.

of 1270 K and 2652 K, respectively), so we do not expect the calculated line fluxes to be much affected. We note here that although Tables 3 and 4 list only pairs of detected $H_2^{16}O$ and $H_2^{17}O$, many $H_2^{16}O$ lines with no accompanying less abundant isotopologue are detected. The full list of all the lines detected and plots of the PACS spectra observed can be found in Appendix C and E, respectively.

3.4. H_2O isotopologues

In all cases, we also searched for the presence of $H_2^{18}O$ in the HIFI, SPIRE and PACS spectra. It is clear that in the HIFI spectra where line blending is not an issue, the 3_{12}–3_{03} transition at 1095.627 GHz is below the noise limit (Fig. 1). In PACS and SPIRE spectra, portions containing isolated unblended transition with another possible lines have been carefully looked at, but there is no emission detected above the noise. With these results, we conclude that our sample of extreme OH/IR star spectra lacks the presence of $H_2^{18}O$. The upper limit of the $H_2^{18}O/H_2^{17}O$ line ratios are given in Appendix A. Here, it is clear that the ratios are below unity in cases where $H_2^{17}O$ lines are detected above the noise. In the sample of oxygen-rich AGB stars from the guaranteed time program HIFISTARS with a lower mass-loss rate, with the same frequency settings as for the OH/IR stars observed in our open-time program (Justtanont et al. 2012), the line fluxes of $H_2^{18}O$ are always brighter than those of $H_2^{17}O$ for both the 1_{11}–0_{00} and 3_{12}–3_{03} transitions (Fig. 5).

The absence of $H_2^{18}O$ in these stars is counter-intuitive considering the observed isotopic ratio of $^{18}O/^{17}O \sim 3$ in the interstellar medium. However, calculations of nucleosynthesis during the AGB phase for intermediate-mass stars predict that for stars with an initial mass larger than 5 $M_\odot$, the temperature at the base of the convective layer is high enough to start hot-bottom burning, preventing the star from becoming a carbon star (see e.g., Lattanzio et al. 1996; Lattanzio & Wood 2003). At the beginning of hot-bottom burning, ^{18}O is destroyed while the production of ^{17}O is increased by an order of magnitude, hence the $^{18}O/^{17}O$ ratio has an expected value of 10^{-6} while the $^{16}O/^{17}O$ ratio is expected to be $\leq$350 (Lattanzio et al. 1996). Hot-bottom burning will finally cease when the star loses most of its mass such that the envelope mass is below 1 $M_\odot$. However, the third dredge-up can still continue and will change the $^{12}C/^{13}C$ ratio while leaving isotopic ratios of other elements almost unaffected. Studies of pre-solar grains reveal very few grains with extremely low $^{18}O/^{16}O$ ratios, which can possibly come from intermediate-mass AGB stars (Lugaro et al. 2007; Nittler et al. 2010), while most of the grains show oxygen isotopic ratios commonly expected from low-mass stars. The rarity of these presolar grains with low ^{18}O content is consistent with the expected population of intermediate-mass stars assuming an initial mass function (Salpeter 1955; Scalo 1986) and the relatively short lifetimes of such stars.

The line flux ratios of $H_2^{16}O/H_2^{17}O$ vary between about unity and less than 10 where the corresponding transition of both

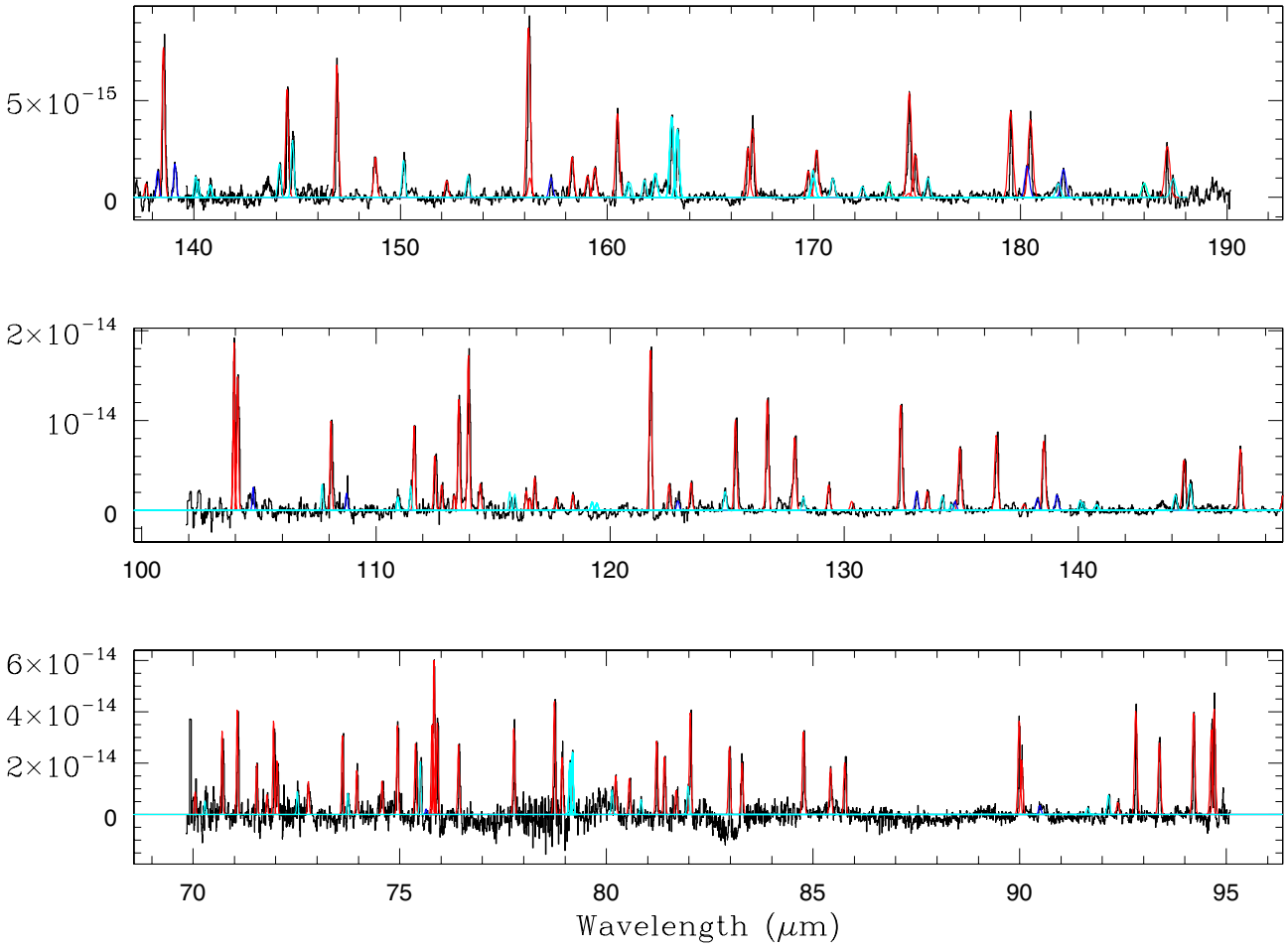

Fig. 4. The continuum subtracted PACS spectrum of AFGL 5379 (histogram) corrected to the ISO-LWS flux level with the Gaussian fits for H_2O (red) and $H_2^{17}O$ (blue). Other molecules are shown in cyan.

molecules is detected (Tables 3 and 4). Most of our reliable line flux ratios from HIFI give values between 2 and 5. This clearly indicates that at least the main line is optically thick. In order to derive isotopic abundance ratio from our observations, a radiative transfer calculation must be performed, which will be addressed in a forthcoming paper.

4. Summary

The H_2O line fluxes observed with *Herschel* are presented for a sample of nine extreme OH/IR stars. These stars are close to the galactic plane and are thought to be population I stars. They all show strong H_2O emission from the main isotopologue and from $H_2^{17}O$. The absence of $H_2^{18}O$ detection was unexpected considering the solar and galactic ratio of $^{18}O/^{17}O$ of 3–5 (Wilson & Rood 1994; Wouterloot et al. 2008).

To explain this question, we propose that our sample stars have undergone hot-bottom burning, which preferentially destroys ^{18}O relative to the other two isotopes. During hot-bottom burning, the abundance of ^{17}O is expected to go up by an order of magnitude while the ^{18}O abundance drops by more than two orders of magnitude. For such a process to happen, the bottom of the convective layer is required to be hotter than 80×10^6 K. This high temperature can be achieved in stars with initial masses of at least 5 $M_\odot$ (Karakas & Lattanzio 2014). It should be noted that hot-bottom burning ceases when the star loses sufficient mass that the high temperature cannot be maintained. Although the isotopic ratios of most elements remain the same after this cessation, the ^{12}C abundance can increase thanks to the continuation of the third dredge-up process bringing up carbon made by the triple-alpha reaction. The materials expelled from these stars will have an impact on local isotopic ratios and may also affect the overall chemical evolution of the Galaxy.

The *Herschel* observations of OH/IR stars complement previous optical ground based AGB star observations of the ^7Li line by García-Hernández et al. (2013), which provides another indication of the operation of the hot-bottom burning in intermediate-mass stars. It may also be possible to search for signatures of hot-bottom burning using elements synthesized during this phase, such as ^{22}Ne and ^{25}Mg. Observations of isotopic ratios of various elements together with theoretical calculations of nucleosynthesis can yield better constraints on the initial mass of these stars.

Acknowledgements. This research is partly funded by the Swedish National Space Board. We also thank both the referee and the editor for further comments for improvement of this paper. HIFI has been designed and built by a consortium of institutes and university departments from across Europe, Canada and the United States under the leadership of SRON Netherlands Institute for Space Research, Groningen, The Netherlands and with major contributions from Germany, France and the US. Consortium members are: Canada: CSA, U.Waterloo; France: CESR, LAB, LERMA, IRAM; Germany: KOSMA, MPIfR, MPS; Ireland, NUI Maynooth; Italy: ASI, IFSI-INAF, Osservatorio Astrofisico di Arcetri-INAF; Netherlands: SRON, TUD; Poland: CAMK, CBK; Spain: Observatorio Astronómico Nacional (IGN), Centro de Astrobiología (CSIC-INTA). Sweden: Chalmers University of Technology – MC2, RSS & GARD; Onsala Space Observatory; Swedish National Space

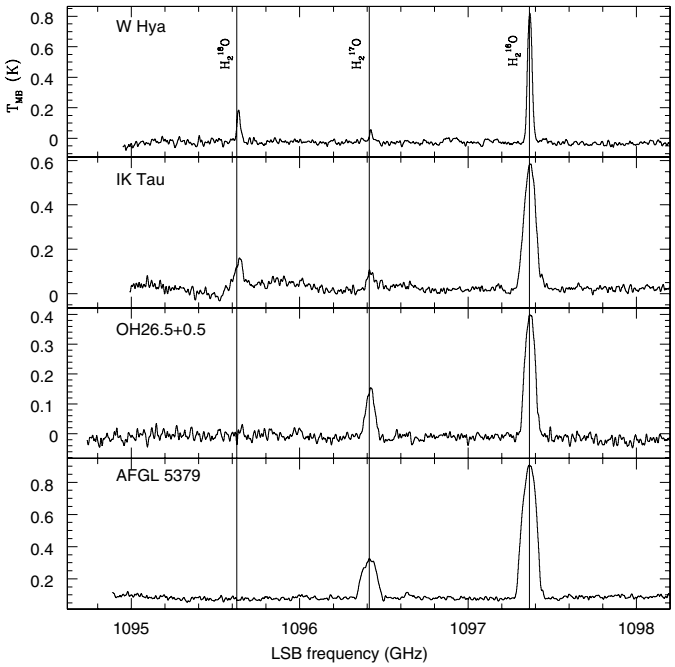

Fig. 5. Observations taken from the HIFISTARS sample showing the $3_{12}-3_{03}$ transition of ortho-H_2O (see Fig. 1). The $H_2^{18}O$ line is clearly detected in W Hya and IK Tau (Justtanont et al. 2012) which have much lower mass-loss rates than in AFGL 5379 and OH 26.5+0.6 (Justtanont et al. 2013).

Board, Stockholm University – Stockholm Observatory; Switzerland: ETH Zurich, FHNW; USA: Caltech, JPL, NHSC. PACS has been developed by a consortium of institutes led by MPE (Germany) and including UVIE (Austria); KU Leuven, CSL, IMEC (Belgium); CEA, LAM (France); MPIA (Germany); INAF-IFSI/OAA/OAP/OAT, LENS, SISSA (Italy); IAC (Spain). This development has been supported by the funding agencies BMVIT (Austria), ESA-PRODEX (Belgium), CEA/CNES (France), DLR (Germany), ASI/INAF (Italy), and CICYT/MCYT (Spain). SPIRE has been developed by a consortium of institutes led by Cardiff University (UK) and including Univ. Lethbridge (Canada); NAOC (China); CEA, LAM (France); IFSI, Univ. Padua (Italy); IAC (Spain); Stockholm Observatory (Sweden); Imperial College London, RAL, UCL-MSSL, UKATC, Univ. Sussex (UK); and Caltech, JPL, NHSC, Univ. Colorado (USA). This development has been supported by national funding agencies: CSA (Canada); NAOC (China); CEA, CNES, CNRS (France); ASI (Italy); MCINN (Spain); SNSB (Sweden); STFC and UKSA (UK); and NASA (USA).

References

Busso, M., Gallino, R., & Wasserburg, G. J. 1999, ARA&A, 37, 239
Clegg, P. E., Ade, P. A. R., Armand, C., et al. 1996, A&A, 315, L38
de Graauw, T., Helmich, F. P., Phillips, T. G., et al. 2010, A&A, 518, L6
García-Hernández, D. A., García-Lario, P., Plez, B., et al. 2007, A&A, 462, 711
García-Hernández, D. A., Zamora, O., Yagüe, A., et al. 2013, A&A, 555, L3
Groenewegen, M. A. T., Waelkens, C., Barlow, M. J., et al. 2011, A&A, 526, A162
Habing, H. J. 1996, A&ARv, 7, 97
Herwig, F. 2005, ARA&A, 43, 435
Iben, Jr., I., & Renzini, A. 1983, ARA&A, 21, 271
Justtanont, K., Skinner, C. J., Tielens, A. G. G. M., Meixner, M., & Baas, F. 1996, ApJ, 456, 337
Justtanont, K., Olofsson, G., Dijkstra, C., & Meyer, A. W. 2006, A&A, 450, 1051
Justtanont, K., Khouri, T., Maercker, M., et al. 2012, A&A, 537, A144
Justtanont, K., Teyssier, D., Barlow, M. J., et al. 2013, A&A, 556, A101
Karakas, A. I., & Lattanzio, J. C. 2014, PASA, 31, 30
Karakas, A. I., García-Hernández, D. A., & Lugaro, M. 2012, ApJ, 751, 8
Kessler, M. F., Steinz, J. A., Anderegg, M. E., et al. 1996, A&A, 315, L27
Lattanzio, J., & Wood, P. R. 2003, in Asymptotic giant branch stars (Berlin, New York: Springer), eds. H. J. Habing, & H. Olofsson, Astron. Astrophysics Lib., 23
Lattanzio, J., Frost, C., Cannon, R., & Wood, P. R. 1996, Mem. Soc. Astron. It., 67, 729
Lombaert, R., Decin, L., de Koter, A., et al. 2013, A&A, 554, A142
Lugaro, M., Karakas, A. I., Nittler, L. R., et al. 2007, A&A, 461, 657
Nittler, L. R., Gyngard, F., & Zinner, E. 2010, Meteorit. Planet. Sci. Suppl., 73, 5245
Ott, S. 2010, in Astronomical Data Analysis Software and Systems XIX, eds. Y. Mizumoto, K.-I. Morita, & M. Ohishi, ASP Conf. Ser., 434, 139
Pilbratt, G. L., Riedinger, J. R., Passvogel, T., et al. 2010, A&A, 518, L1
Sackmann, I.-J., & Boothroyd, A. I. 1992, ApJ, 392, L71
Salpeter, E. E. 1955, ApJ, 121, 161
Scalo, J. M. 1986, Fund. Cosmic Phys., 11, 1
Sylvester, R. J., Barlow, M. J., Nguyen-Q-Rieu, et al. 1997, MNRAS, 291, L42
Wilson, T. L., & Rood, R. 1994, ARA&A, 32, 191
Wood, P. R., Habing, H. J., & McGregor, P. J. 1998, A&A, 336, 925
Wouterloot, J. G. A., Henkel, C., Brand, J., & Davis, G. R. 2008, A&A, 487, 237

Pages 8 to 38 are available in the electronic edition of the journal at http://www.aanda.org

Table 3. Line fluxes of isotopologues of H_2O in the observed SPIRE range.

$\lambda(\mu m)$	Transition	Isotope	Line fluxes ($\times 10^{-17}$ W m^{-2})								
			OH127	GL5379	OH21.5	OH26.5	OH30.7	OH30.1	OH32.0	OH32.8	OH42.3
208.0763	$7_{26}-6_{33}$	16	1.0	14.1	<0.3[a]	5.2	<0.7[a]	1.3	<0.3[a]	0.9	0.7
208.2052	$7_{26}-6_{33}$	17	<0.2[a]	<0.8[a]	<0.3[a]	<0.4[a]	<0.7[a]	<0.3[a]	<0.3[a]	<0.6[a]	<0.4[a]
212.5256	$5_{23}-5_{14}$	16	4.1	57.9	1.8	14.3	<0.7[a]	9.0	2.0	5.3	2.3
213.1557	$5_{23}-5_{14}$	17	1.5	20.2	1.0	7.3	<0.7[a]	2.6	0.8	2.2	1.7
226.7608	$6_{25}-5_{32}$	16	1.7	18.9	0.7	7.4	<0.7[a]	2.3	0.5	2.0	1.3
225.0480	$6_{25}-5_{32}$	17	<0.2[a]	<0.8[a]	<0.3[a]	<0.4[a]	<0.7[a]	<0.3[a]	<0.3[a]	<0.6[a]	<0.4[a]
231.2480[b]	$8_{27}-7_{34}$	16	1.3	12.4	<0.3[a]	3.1	<0.7[a]	<0.3[a]	0.5	1.3	2.1
233.7153	$8_{27}-7_{34}$	17	<0.2[a]	<0.8[a]	<0.3[a]	<0.4[a]	<0.7[a]	<0.3[a]	<0.3[a]	<0.6[a]	<0.4[a]
234.5306	$7_{43}-6_{52}$	16	0.8	9.5	<0.3[a]	5.0	<0.7[a]	1.2	0.5	1.3	<0.4[a]
226.1507	$7_{43}-6_{52}$	17	<0.2[a]	<0.8[a]	<0.3[a]	<0.4[a]	<0.7[a]	<0.3[a]	<0.3[a]	<0.6[a]	<0.4[a]
243.9740	$2_{20}-2_{11}$	16	2.8	31.5	0.7	11.1	<0.7[a]	4.6	0.5	3.4	<0.4[a]
247.1536	$2_{20}-2_{11}$	17	1.6	8.7	<0.3[a]	3.0	<0.7[a]	0.5	<0.3[a]	<0.6[a]	<0.4[a]
248.2468	$4_{22}-4_{13}$	16	3.2	51.8	1.4	10.8	<0.7[a]	6.1	1.1	4.3	1.3
250.3256[b]	$4_{22}-4_{13}$	17	1.3	5.2	<0.3[a]	2.2	<0.7[a]	1.4	<0.3[a]	0.6	<0.4[a]
257.7948	$3_{21}-3_{12}$	16	4.6	66.6	2.4	16.6	0.6	8.7	2.2	6.6	1.2
260.9215	$3_{21}-3_{12}$	17	1.1	11.4	<0.3[a]	3.5	<0.7[a]	1.2	1.4	0.7	<0.4[a]
258.8158	$6_{34}-5_{41}$	16	3.3	11.1	<0.3[a]	4.1	<0.7[a]	1.2	<0.3[a]	<0.6[a]	<0.4[a]
252.0495	$6_{34}-5_{41}$	17	<0.2[a]	<0.8[a]	<0.3[a]	<0.4[a]	<0.7[a]	<0.3[a]	<0.3[a]	<0.6[a]	<0.4[a]
259.9823	$3_{12}-2_{21}$	16	3.1	26.8	0.6	7.6	1.7	3.5	1.9	4.1	1.1
256.6420	$3_{12}-2_{21}$	17	2.2	17.4	<0.3[a]	6.2	<0.7[a]	<0.3[a]	<0.3[a]	1.8	0.6
269.2724	$1_{11}-0_{00}$	16	2.2	23.2	<0.3[a]	8.6	<0.7[a]	3.6	<0.3[a]	1.7	<0.4[a]
270.7745	$1_{11}-0_{00}$	17	1.4	11.4	<0.3[a]	4.1	<0.7[a]	1.2	<0.3[a]	0.8	<0.4[a]
273.1931	$3_{12}-3_{03}$	16	3.6	36.0	2.2	12.1	<0.7[a]	4.1	1.3	5.2	0.9
273.4300	$3_{12}-3_{03}$	17	0.5	12.7	<0.3[a]	1.9	<0.7[a]	2.9	0.6	<0.6[a]	<0.4[a]
303.4562[b]	$2_{02}-1_{11}$	16	2.5	22.6	<0.3[a]	7.8	<0.7[a]	3.1	1.0	2.3	<0.4[a]
302.3565[b]	$2_{02}-1_{11}$	17	1.2	14.9	<0.3[a]	5.2	<0.7[a]	3.1	<0.3[a]	2.3	<0.4[a]
308.9641	$5_{24}-4_{31}$	16	0.6	9.9	<0.3[a]	5.6	<0.7[a]	3.0	<0.3[a]	2.8	2.9
303.4711[b]	$5_{24}-4_{31}$	17	<0.2[a]	<0.8[a]	<0.3[a]	<0.4[a]	<0.7[a]	<0.3[a]	<0.3[a]	<0.6[a]	<0.4[a]
327.2231	$4_{22}-3_{31}$	16	0.8	13.2	2.7	5.9	<0.7[a]	3.7	4.3	5.6	6.0
317.2905	$4_{22}-3_{31}$	17	<0.2[a]	<0.8[a]	<0.3[a]	<0.4[a]	<0.7[a]	<0.3[a]	<0.3[a]	<0.6[a]	<0.4[a]
398.6427	$2_{11}-2_{02}$	16	1.4	20.5	1.8	5.9	1.4	2.8	1.9	2.4	<0.4[a]
400.5467	$2_{11}-2_{02}$	17	0.7	6.7	1.0	2.3	1.4	1.2	1.4	1.2	<0.4[a]
482.9902[b]	$5_{32}-4_{41}$	16	0.4	3.2	0.6	1.3	6.7	<0.3[a]	2.1	0.8	<0.4[a]
455.2615[b]	$5_{32}-4_{41}$	17	<0.2[a]	<0.8[a]	<0.3[a]	<0.4[a]	<0.7[a]	<0.3[a]	<0.3[a]	<0.6[a]	<0.4[a]
538.2890	$1_{10}-1_{01}$	16	0.9	6.9	<0.3[a]	1.3	<0.7[a]	0.8	0.7	0.6	<0.4[a]
543.0817[b]	$1_{10}-1_{01}$	17	0.8	4.6	<0.3[a]	<0.4[a]	0.7	0.5	0.7	<0.6[a]	<0.4[a]

Notes. [(a)] An upper limit of the detection. [(b)] Possible blend with another line.

Table 4. Line fluxes of isotopologues of H_2O in the observed PACS range.

$\lambda(\mu m)$	Transition	Isotope	Line fluxes ($\times 10^{-17}$ W m^{-2})					
			GL5379	OH26.5	OH30.1	OH32.0	OH32.8	OH42.3
57.6365	$4_{22}-3_{13}$	16	115.2	57.8	10.6	<1.6[a]	4.6	<2.7[a]
57.7447[b]	$4_{22}-3_{13}$	17	<36.5[a]	41.1	<4.4[a]	<1.6[a]	<3.1[a]	<2.7[a]
67.0892[b]	$3_{31}-2_{20}$	16	133.5	79.1	16.3	5.7	19.0	4.6
67.5081[b]	$3_{31}-2_{20}$	17	<13.8[a]	16.0	<4.4[a]	<1.6[a]	<3.1[a]	<2.0[a]
75.3807	$3_{21}-2_{12}$	16	135.3	55.7	13.7	3.9	8.2	7.3
75.6381	$3_{21}-2_{12}$	17	<25.9[a]	28.3	<4.4[a]	3.3	0.4	<1.9[a]
75.9099	$5_{50}-5_{41}$	16	177.1	74.1	23.7	8.6	20.9	7.7
76.7892	$5_{50}-5_{41}$	17	<25.9[a]	20.0	<4.4[a]	<1.6[a]	<2.1[a]	<1.9[a]
89.9884	$3_{22}-2_{11}$	16	254.5	84.0	33.3	12.4	22.5	12.9
90.4885	$3_{22}-2_{11}$	17	<24.7[a]	14.2	7.9	2.5	<2.1[a]	6.6
108.0732	$2_{21}-1_{10}$	16	100.1	34.0	9.5	3.7	6.6	2.0
108.7449	$2_{21}-1_{10}$	17	19.4	19.5	3.1	2.8	4.0	<0.7[a]
121.7217	$4_{32}-4_{23}$	16	227.9	70.5	25.4	7.7	17.2	7.0
122.8999	$4_{32}-4_{23}$	17	13.6	10.9	4.2	2.1	2.5	<0.4[a]
132.4084	$4_{23}-4_{14}$	16	176.8	50.6	17.8	8.3	13.2	3.5
133.0943	$4_{23}-4_{14}$	17	31.0	11.6	3.3	1.6	2.3	<0.4[a]
134.9353	$5_{14}-5_{05}$	16	109.2	36.7	13.2	5.4	9.4	3.4
134.7376	$5_{14}-5_{05}$	17	15.5	9.9	<1.0[a]	<0.5[a]	2.3	<0.4[a]
136.4960	$3_{30}-3_{21}$	16	133.9	37.1	12.5	5.8	9.1	3.0
138.2514	$3_{30}-3_{21}$	17	22.4	12.9	1.5	<0.5[a]	1.7	1.7
138.5278	$3_{13}-2_{02}$	16	128.1	45.0	13.7	6.0	9.7	3.5
139.0864	$3_{13}-2_{02}$	17	28.9	17.2	3.8	2.8	3.0	<0.4[a]
156.1940[b]	$3_{22}-3_{13}$	16	184.1	63.7	20.9	10.0	13.8	5.0
157.2836	$3_{22}-3_{13}$	17	22.0	11.9	1.8	<0.9[a]	<0.9[a]	<0.5[a]
156.2652[b]	$5_{23}-4_{32}$	16	21.1	21.5	2.1	3.5	2.1	1.0
153.8758	$5_{23}-4_{32}$	17	<5.6[a]	<4.1[a]	<1.0[a]	<0.9[a]	<0.6[a]	<0.5[a]
179.5267	$2_{12}-1_{01}$	16	122.8	46.8	10.7	5.9	2.4	<0.5[a]
180.3302	$2_{12}-1_{01}$	17	45.7	32.3	5.3	<0.9[a]	0.7	<0.5[a]
180.4883	$2_{21}-2_{12}$	16	112.3	39.0	11.2	4.4	1.3	2.0
182.0899	$2_{21}-2_{12}$	17	41.5	15.2	<1.0[a]	<0.9[a]	<0.6[a]	1.7

Notes. [(a)] An upper limit of the detection. [(b)] A possible blend with higher excited H_2O line.

Appendix A: Line flux ratios

This section of the appendices shows the line flux ratios of $H_2^{18}O/H_2^{17}O$. We note that since the $H_2^{18}O$ is not detected, we give lower limits to the line ratios. In the case when both isotopologues are not detected, the ratios are set to 1.0.

Table A.1. Line flux ratios of $H_2^{18}O/H_2^{17}O$ observed by *Herschel*-HIFI.

Transition	GL5379	OH26.5	OH30.1	OH32.0	OH32.8
$1_{11}-0_{00}$	<0.1	<0.2	a	a	a
$3_{12}-3_{03}$	<0.1	<0.2	<0.4	<0.4	<0.2

Notes. "a" indicates that the transition is not observed.

Table A.2. Line flux ratios of $H_2^{18}O/H_2^{17}O$ in the observed PACS range.

Transition	GL5379	OH26.5	OH30.1	OH32.0	OH32.8	OH42.3
$4_{22}-3_{13}$	–	<0.3	–	–	–	–
$3_{31}-2_{20}$	–	<0.8	–	–	–	–
$3_{21}-2_{12}$	–	<0.4	–	<0.5	<0.6	–
$5_{50}-5_{41}$	–	<0.6	–	–	–	–
$3_{22}-2_{11}$	<0.7	<0.9	–	<0.6	–	<0.3
$2_{21}-1_{10}$	<0.3	<0.4	<0.3	<0.2	<0.2	–
$4_{32}-4_{23}$	<0.4	<0.6	<0.2	<0.2	<0.4	–
$4_{23}-4_{14}$	<0.2	<0.6	<0.3	<0.3	<0.4	–
$5_{14}-5_{05}$	<0.4	<0.7	–	–	<0.4	–
$3_{30}-3_{21}$	<0.3	<0.5	<0.7	–	<0.5	<0.2
$3_{13}-2_{02}$	<0.2	<0.4	<0.3	<0.2	<0.3	–
$3_{22}-3_{13}$	<0.3	<0.6	<0.6	–	–	–
$5_{23}-4_{32}$	–	–	–	–	–	–
$2_{12}-1_{01}$	<0.1	<0.2	<0.2	–	<0.9	–
$2_{21}-2_{12}$	<0.1	<0.5	–	–	–	<0.3

Notes. The "–" symbol indicates that both $H_2^{18}O$ and $H_2^{17}O$ are not detected.

Table A.3. Ratios of $H_2^{18}O/H_2^{17}O$ line fluxes observed with SPIRE.

Transition	OH127	GL5379	OH21.5	OH26.5	OH30.7	OH30.1	OH32.0	OH32.8	OH42.3
$7_{26}-6_{33}$	–	–	–	–	–	–	–	–	–
$5_{23}-5_{14}$	<0.1	<0.1	–	<0.1	–	<0.1	<0.4	<0.3	<0.2
$6_{25}-5_{32}$	–	–	–	–	–	–	–	–	–
$8_{27}-7_{34}$	–	–	–	–	–	–	–	–	–
$7_{43}-6_{52}$	–	–	–	–	–	–	–	–	–
$2_{20}-2_{11}$	<0.1	<0.1	–	<0.1	–	<0.6	–	–	–
$4_{22}-4_{13}$	<0.2	<0.2	–	<0.2	–	<0.2	–	<1.0	–
$3_{21}-3_{12}$	<0.2	<0.1	–	<0.1	–	<0.3	<0.2	<0.9	–
$6_{34}-5_{41}$	–	–	–	–	–	–	–	–	–
$3_{12}-2_{21}$	<0.1	<0.1	–	<0.1	–	–	–	<0.3	<0.7
$1_{11}-0_{00}$	<0.1	<0.1	–	<0.1	–	<0.3	–	<0.7	–
$3_{12}-3_{03}$	<0.4	<0.1	–	<0.2	–	<0.1	0.5	–	–
$2_{02}-1_{11}$	<0.2	<0.1	–	<0.1	–	<0.1	–	<0.3	–
$5_{24}-4_{31}$	–	–	–	–	–	–	–	–	–
$4_{22}-3_{31}$	–	–	–	–	–	–	–	–	–
$2_{11}-2_{02}$	<0.3	<0.1	<0.3	<0.2	<0.5	<0.3	<0.2	<0.5	–
$5_{32}-4_{41}$	–	–	–	–	–	–	–	–	–
$1_{10}-1_{01}$	<0.3	<0.2	–	–	–	<0.6	<0.4	–	–

Notes. The "–" symbol indicates that both $H_2^{18}O$ and $H_2^{17}O$ are not detected.

Appendix B: Compilation of observed SPIRE line fluxes

We present a table with line fluxes for the SPIRE spectra of extreme OH/IR stars.

Table B.1. Line fluxes of all lines detected in the observed SPIRE range.

Molecules	$\lambda(\mu m)$	Line fluxes ($\times 10^{-17}$ W m^{-2})								
		OH127	GL5379	OH21.5	OH26.5	OH30.7	OH30.1	OH32.0	OH32.8	OH42.3
H_2O $6_{33}-5_{42}$	194.4221	2.2	22.5	<0.3	7.9	<0.7	1.7	1.0	1.7	0.7
CO (13−12)	200.2725	1.1	11.3	<0.3	5.6	<0.7	2.9	1.5	2.7	1.7
H_2O ν_2 $2_{20}-2_{11}$	200.6566	0.5	8.9	1.3	3.7	<0.7	<0.3	1.7	1.8	0.9
H_2O ν_2 $5_{23}-4_{32}$	203.4464	0.7	2.2	<0.3	<0.3	<0.7	<0.3	<0.3	<0.6	<0.4
[N II] $^3P_1-^3P_0$	205.1733	<0.2	10.1	17.4	25.0	38.6	31.2	34.6	20.3	11.5
H_2O $7_{26}-6_{33}$	208.0763	1.0	14.1	<0.3	5.2	<0.7	1.3	<0.3	0.9	0.7
H_2O ν_2 $4_{22}-4_{13}$	210.8308	0.6	7.8	<0.3	3.0	<0.7	<0.3	0.4	0.7	<0.4
H_2O $5_{23}-5_{14}$	212.5256	4.1	57.9	1.8	14.3	<0.7	9.0	2.0	5.3	2.3
$H_2^{17}O$ $5_{23}-5_{14}$	213.1557	1.5	20.2	1.0	7.3	<0.7	2.5	0.8	2.2	1.7
CO (12−11)	216.9273	1.6	13.1	<0.3	6.2	<0.7	2.2	1.6	1.9	1.0
H_2S $3_{22}-2_{11}$	220.9835	1.2	7.2	0.5	4.6	0.8	1.6	1.0	1.2	1.1
H_2O $6_{25}-5_{32}$	226.7608	1.7	18.9	0.7	7.4	<0.7	2.3	0.4	2.0	1.3
H_2S $5_{24}-5_{15}$	227.6838	0.5	2.2	<0.3	4.1	<0.7	0.7	<0.3	<0.6	0.6
H_2S $5_{14}-5_{05}$	227.9266	0.8	5.3	0.5	1.7	0.8	1.7	1.0	0.9	0.7
H_2S $6_{34}-6_{25}$	229.6524	0.7	3.7	<0.3	2.1	1.0	0.7	<0.3	<0.6	<0.4
H_2S $8_{35}-7_{62}$	230.8229	1.8	2.4	<0.3	5.3	<0.7	0.8	<0.3	<0.6	<0.4
H_2S $2_{20}-1_{11}$	231.0607	<0.2	8.7	<0.3	2.7	<0.7	1.7	0.8	1.6	<0.4
H_2O $8_{27}-7_{34}$	231.2480	1.3	12.4	<0.3	3.1	<0.7	<0.3	0.5	1.3	<0.4
H_2S $4_{14}-3_{03}$	233.8997	1.3	10.8	<0.3	5.6	1.6	0.7	0.8	1.7	<0.4
H_2S $4_{40}-3_{13}$	234.1534	1.9	8.9	<0.3	7.2	1.3	1.5	0.4	1.8	1.1
H_2O $7_{43}-6_{52}$	234.5306	0.8	9.5	<0.3	5.0	<0.7	1.2	0.5	1.3	<0.4
CO (11−10)	236.6133	0.8	9.6	<0.3	2.2	<0.7	1.5	0.8	0.8	<0.4
H_2O $2_{20}-2_{11}$	243.9740	2.8	31.5	0.6	11.1	<0.7	4.6	0.5	3.4	<0.4
NH_3 2_1-1_1	246.6929	2.3	20.1	<0.3	5.8	<0.7	1.2	<0.3	0.8	<0.4
$H_2^{17}O$ $2_{20}-2_{11}$	247.1537	1.6	8.6	<0.3	3.0	<0.7	0.5	<0.3	<0.6	<0.4
H_2O $4_{22}-4_{13}$	248.2468	3.2	51.8	1.4	10.8	<0.7	6.0	1.1	4.3	1.3
H_2O ν_2 $4_{22}-4_{13}$	248.6277	1.2	5.7	<0.3	1.5	<0.7	<0.3	<0.3	<0.6	<0.4
$H_2^{17}O$ $3_{12}-2_{21}$	250.3257	1.3	5.2	<0.3	2.2	<0.7	1.4	<0.3	0.6	<0.4
H_2S $3_{12}-2_{21}$	250.6601	0.5	8.2	0.6	6.0	<0.7	0.8	<0.3	0.9	<0.4
NH_3 2_1-1_1	256.5724	0.4	<0.8	0.5	<0.4	<0.7	1.4	<0.3	0.9	<0.4
$H_2^{17}O$ $3_{12}-2_{21}$	256.6420	2.1	17.4	<0.3	6.2	<0.7	<0.3	<0.3	1.8	0.6
H_2O $3_{21}-3_{12}$	257.7947	4.6	66.6	2.4	16.6	<0.7	8.6	2.2	6.6	1.2
H_2O $6_{34}-5_{41}$	258.8158	0.3	11.1	<0.3	4.1	<0.7	1.2	<0.3	<0.6	<0.4
H_2O $3_{12}-2_{21}$	259.9822	3.1	26.8	0.6	7.6	1.7	3.5	1.9	4.1	1.1
CO (10−9)	260.2399	0.8	18.8	0.6	7.9	<0.7	3.5	0.6	1.4	0.7
$H_2^{17}O$ $3_{21}-3_{12}$	260.9215	1.1	11.4	<0.3	3.5	<0.7	1.2	<0.3	0.7	<0.4
H_2O $1_{11}-0_{00}$	269.2724	2.2	23.2	0.5	8.6	<0.7	3.6	<0.3	1.7	<0.4
$H_2^{17}O$ $1_{11}-0_{00}$	270.7744	1.4	11.4	0.6	4.1	<0.7	1.1	<0.3	0.8	<0.4
^{13}CO (10−9)	272.2046	0.7	4.8	<0.3	2.2	<0.7	1.0	<0.3	<0.6	<0.4
H_2O $3_{12}-3_{03}$	273.1931	3.6	36.0	2.2	12.1	<0.7	4.1	1.3	5.2	<0.4
$H_2^{17}O$ $3_{12}-3_{03}$	273.4300	0.4	12.7	<0.3	1.9	<0.7	2.9	0.5	<0.6	0.9
SiO (25−24)	276.6864	<0.1	0.7	<0.3	<0.4	<0.7	<0.3	<0.3	<0.6	<0.4
H_2S $2_{21}-1_{10}$	279.4393	1.0	8.8	<0.3	4.0	<0.7	1.5	<0.3	0.7	<0.4
HCN (12−11)	282.0294	<0.1	1.6	<0.3	<0.4	<0.7	<0.3	<0.3	<0.6	<0.4
SiO (24−23)	288.1664	<0.1	2.9	<0.3	<0.4	<0.7	<0.3	<0.3	<0.6	<0.4
CO (9−8)	289.1205	1.1	9.7	0.4	3.4	<0.7	2.0	<0.3	<0.6	<0.4
H_2S $4_{23}-4_{14}$	292.0500	0.7	4.6	<0.3	3.2	<0.7	1.2	<0.3	<0.6	<0.4
H_2S $3_{13}-2_{02}$	298.9617	0.6	5.7	<0.3	3.7	<0.7	1.7	0.4	<0.6	1.3
SiO (23−22)	300.6476	<0.1	2.5	<0.3	<0.4	<0.7	<0.3	<0.3	<0.6	<0.4
H_2S $3_{03}-2_{11}$	301.8748	1.5	10.2	<0.3	3.9	<0.7	1.3	<0.3	<0.6	<0.4
$H_2^{17}O$ $2_{02}-1_{11}$	302.3565	1.2	14.9	<0.3	5.2	<0.7	3.1	<0.3	2.3	1.2
^{13}CO (9−8)	302.4147	<0.1	2.4	<0.3	1.0	<0.7	2.8	<0.3	<0.6	<0.4
H_2O $2_{02}-1_{11}$	303.4561	2.5	22.6	<0.3	7.8	<0.7	3.1	1.0	2.3	<0.4
HCN (11−10)	307.6410	0.4	3.4	<0.3	<0.4	<0.7	<0.3	<0.3	<0.6	<0.4
H_2O $5_{24}-4_{31}$	308.9641	0.6	9.9	<0.3	5.6	<0.7	3.0	<0.3	2.8	<0.4
SiO (22−21)	314.2667	<0.1	1.3	<0.3	<0.4	<0.7	<0.3	<0.3	<0.6	<0.4
CO (8−7)	325.2251	1.1	9.5	2.3	3.7	5.5	3.4	2.5	4.4	3.0
H_2O $4_{22}-3_{31}$	327.2230	0.8	13.2	2.7	5.9	<0.7	3.7	4.3	5.6	6.0

Table B.1. continued.

Molecules	$\lambda(\mu m)$	Line fluxes ($\times 10^{-17}$ W m^{-2})								
		OH127	GL5379	OH21.5	OH26.5	OH30.7	OH30.1	OH32.0	OH32.8	OH42.3
SiO (21–10)	329.1855	<0.1	2.2	<0.3	<0.4	<0.7	<0.3	<0.3	<0.6	<0.4
H_2O ν_2 $2_{20}-1_{11}$	333.3613	0.7	1.9	<0.3	<0.4	<0.7	<0.3	<0.3	<0.6	<0.4
HCN (10–9)	338.3773	0.3	<0.8	<0.3	<0.4	<0.7	<0.3	<0.3	<0.6	<0.4
^{13}CO (8–7)	340.1812	0.4	3.4	<0.3	1.3	<0.7	<0.3	<0.3	<0.6	<0.4
SiO (20–19)	345.5993	<0.1	0.9	<0.3	<0.4	<0.7	<0.3	<0.3	<0.6	<0.4
H_2S $6_{61}-6_{52}$	348.5420	0.5	<0.8	<0.3	1.6	<0.7	1.6	<0.3	<0.6	<0.4
H_2O ν_2 $2_{11}-2_{02}$	348.6097	0.5	5.2	<0.3	<0.4	<0.7	<0.3	<0.3	<0.6	<0.4
H_2S $6_{52}-6_{43}$	350.6485	0.3	<0.8	<0.3	3.2	<0.7	2.2	<0.3	<0.6	<0.4
SiO (19–18)	363.7438	<0.1	1.5	<0.3	<0.4	<0.7	<0.3	<0.3	<0.6	<0.4
[C I] (2–1)	370.4142	0.7	1.4	3.3	4.6	11.8	3.0	5.1	4.3	13.2
CO (7–6)	371.6504	0.6	7.8	<0.3	0.8	<0.7	0.7	<0.3	0.7	<0.4
HCN (9–8)	375.9465	<0.1	0.7	<0.3	<0.4	<0.7	<0.3	<0.3	<0.6	<0.4
SiO (18–17)	383.9074	<0.1	1.4	<0.3	<0.4	<0.7	<0.3	<0.3	<0.6	<0.4
^{13}CO (7–6)	388.7432	0.3	3.6	<0.3	<0.4	<0.7	<0.3	<0.3	<0.6	<0.4
H_2O $2_{11}-2_{02}$	398.6428	1.4	20.5	1.8	5.9	1.4	2.8	1.9	2.4	1.4
$H_2^{17}O$ $2_{11}-2_{02}$	400.5469	0.7	6.7	0.9	2.3	1.4	1.2	1.4	1.2	1.7
SiO (17–16)	406.4465	<0.1	2.2	<0.3	<0.4	<0.7	<0.3	<0.3	<0.6	<0.4
H_2S $2_{12}-1_{01}$	407.3080	0.9	7.0	1.3	2.2	4.7	2.5	2.1	3.0	<0.4
HCN (8–7)	422.9119	0.2	1.8	<0.3	0.3	<0.7	<0.3	<0.3	<0.6	<0.4
SiO (16–15)	431.8066	<0.1	1.6	<0.3	<0.4	<0.7	<0.3	<0.3	<0.6	<0.4
CO (6–5)	433.5563	0.7	6.2	<0.3	2.3	1.9	1.5	1.4	1.5	<0.4
H_2S $2_{02}-1_{11}$	436.1862	0.6	4.1	0.4	1.9	<0.7	0.4	<0.3	<0.6	<0.4
^{13}CO (6–5)	453.4979	0.6	3.1	<0.3	1.1	<0.7	0.4	<0.3	<0.6	<0.4
H_2O ν_2 $1_{10}-1_{01}$	455.6076	0.2	1.2	1.0	1.0	<0.7	<0.3	<0.3	<0.6	<0.4
SiO (15–14)	460.5504	<0.1	1.2	<0.3	0.7	<0.7	<0.3	<0.3	<0.6	<0.4
H_2O $5_{32}-4_{41}$	482.9902	0.4	3.2	0.6	1.3	<0.7	<0.3	<0.3	0.8	<0.4
HCN (7–6)	483.2993	0.1	0.3	<0.3	1.4	<0.7	<0.3	<0.3	<0.6	<0.4
SiO (14–13)	493.4052	<0.1	1.3	<0.3	<0.4	<0.7	<0.3	<0.3	<0.6	<0.4
H_2S $5_{50}-5_{41}$	517.0628	<0.1	1.2	0.8	<0.4	<0.7	0.3	<0.3	<0.6	<0.4
CO (5–4)	520.2311	0.9	5.9	2.4	4.0	6.3	1.7	3.3	3.4	2.2
NH_3 1_0-0_0	523.6569	0.4	1.0	<0.3	1.0	<0.7	<0.3	<0.3	<0.6	<0.4
SiO (13–12)	531.3171	<0.1	1.0	<0.3	0.6	<0.7	<0.3	<0.3	<0.6	<0.4
H_2O $1_{10}-1_{01}$	538.2890	0.9	6.9	<0.3	1.3	<0.7	0.8	0.7	0.6	<0.4
$H_2^{17}O$ $1_{10}-1_{01}$	543.0817	0.8	4.5	<0.3	<0.4	<0.7	0.5	0.7	<0.6	<0.4
HCN (6–5)	563.8207	<0.1	0.4	<0.3	<0.4	<0.7	<0.3	<0.3	<0.6	<0.4
SiO (11–10)	575.5523	<0.1	0.7	<0.3	<0.4	<0.7	<0.3	<0.3	<0.6	<0.4
[C I] (1–0)	609.1350	1.7	2.0	5.0	8.1	17.6	5.9	6.6	7.1	13.2
CO (4–3)	650.2513	<0.1	5.2	2.9	5.1	17.0	3.7	7.1	7.6	7.5

Appendix C: Compilation of observed PACS line fluxes

We present tables for the list of lines detected in the PACS spectra for individual objects.

Table C.1. Line fluxes calculated from PACS spectra of AFGL 5379.

Molecules	$\lambda(\mu m)$	F_{line} ($\times 10^{-17}$ W m^{-2})
H_2O $4_{31}-3_{22}$	56.3250	88.9 ± 35.6
H_2O $4_{22}-3_{13}$	57.6365	155.2 ± 57.4
H_2O $4_{32}-3_{21}$	58.6991	166.6 ± 38.7
H_2O $8_{26}-7_{35}$	60.1622	78.5 ± 40.7
H_2O $6_{60}-6_{51}$	63.9281	164.5 ± 45.9
H_2O $9_{64}-9_{55}$	63.9940	81.6 ±141.5
H_2O $6_{25}-5_{14}$	65.1662	161.0 ± 14.7
H_2O $10_{38}-10_{29}$	65.5763	96.2 ± 14.9
H_2O $7_{16}-6_{25}$	66.0927	123.4 ± 18.1
H_2O $3_{30}-2_{21}$	66.4377	74.5 ± 18.3
H_2O $3_{31}-2_{20}$	67.0892	133.5 ± 18.7
H_2O $3_{30}-3_{03}$	67.2690	134.3 ± 18.8
H_2O $11_{57}-11_{48}$	70.0500	36.7 ± 17.0
H_2O ν_2 $3_{21}-2_{12}$	70.2871	22.1 ± 17.1
H_2O $8_{27}-8_{18}$	70.7026	139.9 ± 17.3
H_2O $5_{24}-4_{13}$	71.0673	177.6 ± 17.5
H_2O $7_{17}-6_{06}$	71.5397	86.4 ± 17.7
H_2O $5_{51}-6_{24}$	71.7878	33.8 ± 17.8
H_2O $7_{07}-6_{16}$	71.9470	162.5 ± 17.9
H_2O $8_{17}-8_{08}$	72.0323	93.7 ± 17.9
H_2O $10_{56}-10_{47}$	72.7893	59.0 ± 18.3
H_2O $9_{37}-9_{28}$	73.6129	143.9 ± 18.7
H_2O ν_2 $4_{23}-3_{12}$	73.7448	38.5 ± 18.8
H_2O $10_{47}-10_{38}$	73.9603	80.9 ± 18.9
H_2O $9_{55}-9_{46}$	74.5735	62.6 ± 19.2
H_2O $7_{25}-6_{34}$	74.9450	168.2 ± 19.4
H_2O $3_{21}-2_{12}$	75.3807	135.3 ± 24.5
H_2O [a] $5_{51}-5_{42}$	75.7814	173.2 ± 24.8
H_2O [a] $7_{53}-7_{44}$	75.8134	99.3 ± 24.8
H_2O [a] $6_{52}-6_{43}$	75.8300	298.2 ± 24.8
H_2O $5_{50}-5_{41}$	75.9099	177.1 ± 24.9
H_2O $6_{51}-6_{42}$	76.4220	136.7 ± 25.2
H_2O $7_{52}-7_{43}$	77.7615	174.8 ± 26.1
H_2O $4_{23}-3_{12}$	78.7424	235.9 ± 26.8
H_2O $6_{15}-5_{24}$	78.9285	119.0 ± 26.9
OH $^2\Pi_{1/2}$ 1/2–$^2\Pi_{3/2}$ 3/2	79.1173	108.9 ± 27.0
OH $^2\Pi_{1/2}$ 1/2–$^2\Pi_{3/2}$ 3/2	79.1809	131.2 ± 27.1
H_2O $9_{46}-9_{37}$	80.2223	83.4 ± 23.4
H_2O $8_{53}-8_{44}$	80.5568	78.2 ± 23.5
H_2O $7_{26}-7_{17}$	81.2156	162.2 ± 23.9
H_2O $9_{27}-9_{18}$	81.4054	127.4 ± 24.0
H_2O $8_{35}-7_{44}$	81.6902	54.2 ± 24.2
H_2O ν_2 [a] $6_{16}-5_{05}$	81.9761	64.3 ± 24.4
H_2O [a] $6_{16}-5_{05}$	82.0315	229.6 ± 24.4
H_2O $8_{36}-8_{27}$	82.9767	155.8 ± 25.0
H_2O $6_{06}-5_{15}$	83.2840	119.8 ± 25.2
H_2O $7_{16}-7_{07}$	84.7670	200.1 ± 26.1
H_2O $9_{54}-9_{45}$	85.4248	113.9 ± 17.7
H_2O $8_{45}-8_{36}$	85.7688	128.6 ± 17.8
H_2O $3_{22}-2_{11}$	89.9884	254.5 ± 19.6
H_2O $7_{44}-7_{35}$	90.0498	148.0 ± 19.6
H_2O ν_2 $2_{20}-1_{11}$	92.1496	55.1 ± 16.9
H_2O $10_{55}-10_{46}$	92.3768	34.0 ± 17.0
H_2O $6_{43}-6_{34}$	92.8108	299.0 ± 17.1
H_2O $7_{35}-7_{26}$	93.3829	209.9 ± 17.3
H_2O $5_{42}-5_{33}$	94.2096	301.4 ± 17.6
H_2O $6_{25}-6_{16}$	94.6441	255.5 ± 17.8
H_2O $4_{41}-4_{32}$	94.7052	318.2 ± 17.8
H_2O [a] $6_{42}-6_{33}$	103.9163	93.3 ± 13.1
H_2O [a] $6_{15}-6_{06}$	103.9402	173.8 ± 13.1
H_2O $6_{34}-6_{25}$	104.0937	139.0 ± 13.1
H_2O $2_{21}-1_{10}$	108.0732	100.1 ± 14.1

Notes. [(a)] The line is blended with a nearby transition.

Table C.1. continued.

Molecules	$\lambda(\mu m)$	F_{line} ($\times 10^{-17}$ W m^{-2})
$H_2^{17}O$ $2_{21}-1_{10}$	108.7449	19.4 ± 14.3
H_2S^a $8_{27}-7_{16}$	110.9346	15.9 ± 8.0
H_2S^a $8_{17}-7_{26}$	110.9364	15.9 ± 8.0
H_2O ν_2 $4_{14}-3_{03}$	111.4826	29.2 ± 8.1
H_2O $5_{24}-5_{15}$	111.6280	100.8 ± 8.1
H_2O $7_{43}-7_{34}$	112.5106	66.4 ± 8.2
H_2O $4_{41}-5_{14}$	112.8029	31.1 ± 8.2
H_2O $4_{14}-3_{03}$	113.5374	137.3 ± 8.4
H_2O $5_{33}-5_{24}$	113.9480	193.4 ± 8.4
H_2O $9_{27}-10_{1*}$	114.4537	33.3 ± 8.5
H_2O $7_{34}-6_{43}$	116.7791	43.2 ± 7.1
H_2O $9_{37}-8_{44}$	118.4053	21.4 ± 7.3
OH $^2\Pi_{3/2}$ 5/2-3/2	119.2325	−11.9 ± 7.4
OH $^2\Pi_{3/2}$ 5/2-3/2	119.4417	−9.8 ± 7.4
H_2O $4_{32}-4_{23}$	121.7217	227.9 ± 7.7
H_2O $8_{44}-8_{35}$	122.5222	37.4 ± 7.8
H_2O $9_{36}-9_{27}$	123.4605	40.2 ± 7.9
NH_3 $4_{01}-3_{00}$	124.9125	28.4 ± 8.1
H_2O $4_{04}-3_{13}$	125.3537	136.3 ± 6.8
H_2O $3_{31}-3_{22}$	126.7140	170.2 ± 6.9
H_2O $7_{25}-7_{16}$	127.8842	114.2 ± 7.1
H_2O ν_2 $4_{04}-3_{13}$	128.2586	21.2 ± 7.1
H_2O $9_{45}-9_{36}$	129.3390	40.9 ± 7.2
H_2O $4_{23}-4_{14}$	132.4084	176.8 ± 6.1
$H_2^{17}O$ $4_{23}-4_{14}$	133.0943	31.0 ± 6.1
H_2O $8_{36}-7_{43}$	133.5491	32.4 ± 6.2
H_2O ν_2 $3_{13}-2_{02}$	134.1938	24.6 ± 6.2
H_2O $5_{14}-5_{05}$	134.9353	109.2 ± 6.3
H_2O $3_{30}-3_{21}$	136.4960	133.9 ± 6.4
$H_2^{17}O$ $3_{30}-3_{21}$	138.2514	22.4 ± 6.6
H_2O $3_{13}-2_{02}$	138.5278	128.1 ± 6.6
$H_2^{17}O$ $3_{13}-2_{02}$	139.0864	28.9 ± 6.7
H_2S $5_{23}-4_{32}$	144.1417	31.0 ± 5.4
H_2O $4_{13}-3_{22}$	144.5179	100.6 ± 5.4
H_2S $3_{21}-2_{12}$	144.7797	53.3 ± 5.4
H_2O $4_{31}-4_{22}$	146.9228	127.0 ± 5.6
H_2O $5_{42}-6_{15}$	148.7904	39.4 ± 5.7
H_2S $4_{32}-3_{21}$	150.1524	37.0 ± 5.8
H_2O ν_2 $2_{21}-2_{12}$	153.2704	22.9 ± 6.1
H_2O^a $3_{22}-3_{13}$	156.1940	184.1 ± 6.3
H_2O^a $5_{23}-4_{32}$	156.2652	21.1 ± 6.3
H_2O $3_{31}-4_{04}$	158.3116	44.9 ± 6.5
H_2O $8_{45}-7_{52}$	159.0506	24.3 ± 6.6
H_2O $6_{34}-7_{07}$	159.4003	33.7 ± 6.6
H_2O $5_{32}-5_{23}$	160.5101	95.9 ± 4.5
H_2S $5_{14}-4_{23}$	161.8151	20.4 ± 4.5
OH^a $^2\Pi_{1/2}$ 3/2-1/2	163.1243	95.2 ± 4.6
OH^a $^2\Pi_{1/2}$ 3/2-1/2	163.3972	81.1 ± 4.6
H_2O $7_{34}-7_{25}$	166.8147	61.0 ± 4.1
H_2O $6_{24}-6_{15}$	167.0350	85.0 ± 4.1
H_2O $7_{35}-6_{42}$	169.7388	34.0 ± 4.2
H_2O $6_{33}-6_{24}$	170.1392	60.6 ± 4.8
H_2O ν_2 $2_{12}-1_{01}$	170.9276	24.9 ± 4.8
H_2O ν_2 $4_{13}-4_{04}$	172.3588	14.2 ± 4.9
CO (15−14)	173.6315	19.9 ± 4.9
H_2O^a $5_{33}-6_{06}$	174.6069	5.3 ± 5.0
H_2O^a $3_{03}-2_{12}$	174.6259	142.0 ± 5.0
H_2O $4_{32}-5_{05}$	174.9201	57.5 ± 5.0
H_2S $3_{31}-2_{20}$	175.5257	26.5 ± 5.6
H_2O $2_{12}-1_{01}$	179.5267	122.7 ± 7.0
$H_2^{17}O$ $2_{12}-1_{01}$	180.3302	45.7 ± 7.0
H_2O $2_{21}-2_{12}$	180.4883	112.3 ± 7.0
H_2S $4_{22}-3_{31}$	181.8342	20.6 ± 8.6
$H_2^{17}O$ $2_{21}-2_{12}$	182.0899	41.5 ± 8.6
CO (14−13)	185.9993	22.0 ± 9.0
H_2O $4_{13}-4_{04}$	187.1108	79.7 ± 9.1
H_2S $4_{23}-3_{12}$	187.3993	29.5 ± 9.1

Table C.2. Line fluxes calculated from PACS spectra of OH 26.5+0.6.

Molecules	$\lambda(\mu m)$	F_{line} ($\times 10^{-17}$ W m^{-2})
H_2O $8_{27}-7_{16}$	55.1310	108.2 ± 18.4
H_2O $4_{22}-3_{13}$	57.6365	57.7 ± 14.4
H_2O $4_{32}-3_{21}$	58.6991	76.1 ± 11.9
H_2O $7_{26}-6_{15}$	59.9871	53.7 ± 9.3
H_2O $8_{26}-7_{35}$	60.1622	44.1 ± 9.4
H_2O $4_{31}-4_{04}$	61.8086	83.2 ± 13.2
H_2O $4_{40}-5_{15}$	61.9162	38.0 ± 13.2
H_2O $9_{36}-8_{45}$	62.4179	13.5 ± 13.5
H_2O $9_{28}-9_{19}$	62.4316	62.1 ± 13.5
H_2O $8_{18}-7_{07}$	63.3236	45.8 ± 13.9
H_2O $8_{08}-7_{17}$	63.4580	38.7 ± 13.9
H_2O $6_{60}-6_{51}$	63.9281	95.8 ± 14.1
H_2O $9_{64}-9_{55}$	63.9940	57.4 ± 14.2
H_2O $9_{63}-9_{54}$	64.8990	33.4 ± 14.6
H_2O $6_{25}-5_{14}$	65.1662	78.2 ± 14.7
H_2O $10_{38}-10_{29}$	65.5763	59.0 ± 14.9
H_2O $6_{25}-5_{14}$	65.1662	77.6 ± 14.7
H_2O $10_{38}-10_{29}$	65.5763	60.3 ± 14.9
H_2O $7_{16}-6_{25}$	66.0927	75.2 ± 15.1
H_2O $3_{30}-2_{21}$	66.4377	45.1 ± 15.3
H_2O $3_{31}-2_{20}$	67.0892	79.1 ± 15.6
H_2O $3_{30}-3_{03}$	67.2690	57.2 ± 15.6
H_2O ν_2 $7_{16}-6_{25}$	67.3654	24.3 ± 13.7
$H_2^{17}O$ $3_{31}-2_{20}$	67.5081	16.1 ± 13.8
H_2O $11_{48}-11_{39}$	67.5854	26.5 ± 13.8
H_2O ν_2 $3_{21}-2_{12}$	70.2871	36.7 ± 8.5
H_2O $8_{27}-8_{18}$	70.7026	75.0 ± 8.6
H_2O $5_{24}-4_{13}$	71.0673	76.1 ± 8.7
H_2O $7_{17}-6_{06}$	71.5397	42.5 ± 8.8
H_2O $7_{07}-6_{16}$	71.9470	78.4 ± 8.9
H_2O $8_{17}-8_{08}$	72.0323	47.6 ± 9.0
H_2O ν_2 $7_{07}-6_{16}$	72.5218	9.1 ± 9.1
H_2O $10_{56}-10_{47}$	72.7893	38.7 ± 9.2
H_2O $9_{37}-9_{28}$	73.6129	53.2 ± 9.4
H_2O ν_2 $4_{23}-3_{12}$	73.7448	33.6 ± 9.4
H_2O $10_{47}-10_{38}$	73.9603	40.7 ± 9.5
H_2O $9_{55}-9_{46}$	74.5735	41.0 ± 9.6
H_2O $7_{25}-6_{34}$	74.9450	73.1 ± 9.7
H_2O $3_{21}-2_{12}$	75.3807	55.7 ± 4.9
H_2O $8_{54}-8_{45}$	75.4955	49.7 ± 8.9
$H_2^{17}O$ $3_{21}-2_{12}$	75.6381	28.3 ± 8.9
H_2O $5_{51}-5_{42}$	75.7814	63.0 ± 8.9
H_2O $7_{53}-7_{44}$	75.8134	98.9 ± 8.9
H_2O $6_{52}-6_{43}$	75.8300	133.6 ± 8.9
H_2O $5_{50}-5_{41}$	75.9099	74.1 ± 9.0
H_2O $6_{51}-6_{42}$	76.4220	73.7 ± 9.1
$H_2^{17}O$ $5_{50}-5_{41}$	76.7892	20.0 ± 9.2
H_2O $7_{52}-7_{43}$	77.7615	81.6 ± 9.4
H_2O $4_{23}-3_{12}$	78.7424	84.7 ± 9.6
H_2O $6_{15}-5_{24}$	78.9285	64.6 ± 9.7
OH $^2\Pi_{1/2}$ 1/2$-^2\Pi_{3/2}$ 3/2	79.1173	72.4 ± 9.7
OH $^2\Pi_{1/2}$ 1/2$-^2\Pi_{3/2}$ 3/2	79.1809	88.7 ± 9.8
H_2O ν_2 $4_{41}-4_{32}$	80.1388	36.1 ± 11.1
H_2O $9_{46}-9_{37}$	80.2223	67.7 ± 11.1
H_2O $8_{53}-8_{44}$	80.5568	60.5 ± 11.2
H_2O ν_2 $4_{40}-4_{31}$	80.8397	25.7 ± 11.3
H_2O $7_{26}-7_{17}$	81.2156	70.5 ± 11.4
H_2O $9_{27}-9_{18}$	81.4054	82.6 ± 11.5
H_2O $11_{38}-11_{29}$	81.5934	31.0 ± 11.5
H_2O $8_{35}-7_{44}$	81.6902	48.8 ± 11.5
H_2O ν_2 $6_{16}-5_{05}$	81.9761	22.4 ± 11.6
H_2O $6_{16}-5_{05}$	82.0315	66.0 ± 11.6
H_2O $8_{36}-8_{27}$	82.9767	117.9 ± 11.9
H_2O $6_{06}-5_{15}$	83.2840	93.7 ± 12.0

Notes. [(a)] The line is blended with a nearby transition.

Table C.2. continued.

Molecules	$\lambda(\mu m)$	F_{line} ($\times 10^{-17}$ W m^{-2})
H_2O ν_2 $6_{06}-5_{15}$	84.0679	55.1 ± 12.2
OH $3_{*0}-2_{10}$	84.4200	12.3 ± 12.3
OH $3_{*0}-2_{10}$	84.4204	12.3 ± 12.3
OH $3_{*0}-2_{10}$	84.4204	12.3 ± 12.3
H_2O $7_{16}-7_{07}$	84.7670	89.5 ± 12.4
H_2O $9_{54}-9_{45}$	85.4248	37.4 ± 12.6
H_2O $8_{45}-8_{36}$	85.7688	83.8 ± 14.0
H_2O $3_{22}-2_{11}$	89.9884	84.0 ± 15.4
H_2O $7_{44}-7_{35}$	90.0498	105.1 ± 15.4
$H_2^{17}O$ $3_{22}-2_{11}$	90.4885	14.1 ± 15.6
H_2O ν_2 $2_{20}-1_{11}$	92.1496	47.7 ± 16.9
H_2O $6_{43}-6_{34}$	92.8108	121.6 ± 17.1
H_2O $7_{35}-7_{26}$	93.3829	128.5 ± 17.3
H_2O $5_{42}-5_{33}$	94.2096	95.9 ± 17.6
H_2O $6_{25}-6_{16}$	94.6441	98.8 ± 17.8
H_2O $4_{41}-4_{32}$	94.7052	101.9 ± 17.8
H_2O ν_2 $5_{15}-4_{04}$	94.8966	42.7 ± 17.9
H_2O $6_{42}-6_{33}$	103.9163	76.2 ± 4.7
H_2O $6_{15}-6_{06}$	103.9402	18.7 ± 4.7
H_2O $6_{34}-6_{25}$	104.0937	48.4 ± 3.7
H_2O $12_{57}-12_{48}$	105.2274	7.7 ± 7.7
H_2O ν_2 $3_{31}-3_{22}$	106.7648	13.1 ± 3.9
H_2O $10_{55}-9_{64}$	106.9978	13.5 ± 4.0
H_2O ν_2 $5_{14}-4_{23}$	107.7044	10.6 ± 4.0
H_2O $2_{21}-1_{10}$	108.0732	34.0 ± 4.0
$H_2^{17}O$ $2_{21}-1_{10}$	108.7449	19.5 ± 4.1
H_2O ν_2 $4_{14}-3_{03}$	111.4826	16.1 ± 4.3
H_2O $5_{24}-5_{15}$	111.6280	33.1 ± 4.3
H_2O $7_{43}-7_{34}$	112.5106	34.9 ± 4.4
H_2O $4_{14}-3_{03}$	113.5374	40.8 ± 4.5
H_2O $5_{33}-5_{24}$	113.9480	62.9 ± 4.5
H_2O $9_{27}-10_{1*}$	114.4537	8.9 ± 6.8
H_2O ν_2 $4_{23}-4_{14}$	115.7146	11.0 ± 6.9
H_2O $10_{38}-9_{45}$	116.4241	8.5 ± 7.0
H_2O $11_{47}-11_{38}$	116.5708	8.9 ± 7.0
H_2O $7_{34}-6_{43}$	116.7791	23.3 ± 4.7
H_2O $9_{46}-8_{53}$	117.6840	8.3 ± 4.8
H_2O ν_2 $6_{24}-5_{33}$	117.9483	5.9 ± 4.8
H_2O $9_{37}-8_{44}$	118.4053	10.4 ± 4.8
OH $^2\Pi_{3/2}$ 5/2-3/2	119.2342	8.8 ± 4.9
OH $^2\Pi_{3/2}$ 5/2-3/2	119.4417	8.5 ± 4.9
H_2O $4_{32}-4_{23}$	121.7217	70.5 ± 7.7
H_2O $8_{44}-8_{35}$	122.5222	22.2 ± 7.8
$H_2^{17}O$ $4_{32}-4_{23}$	122.8999	10.9 ± 7.8
H_2O $9_{36}-9_{27}$	123.4605	20.1 ± 7.9
H_2O ν_2 $5_{14}-5_{05}$	124.8494	17.2 ± 8.1
NH_3 $4_{01}-3_{00}$	124.9125	17.2 ± 8.1
H_2O $4_{04}-3_{13}$	125.3537	40.5 ± 5.4
H_2O $3_{31}-3_{22}$	126.7140	50.1 ± 5.5
NH_3 $4_{10}-3_{11}$	127.1811	12.0 ± 5.6
H_2O $7_{25}-7_{16}$	127.8842	40.7 ± 5.7
H_2O ν_2 $4_{04}-3_{13}$	128.2586	16.0 ± 5.7
H_2O $9_{45}-9_{36}$	129.3390	23.9 ± 5.8
H_2O $7_{53}-8_{26}$	130.3187	7.2 ± 5.9
H_2O ν_2 $5_{32}-5_{23}$	130.6752	15.9 ± 5.9
H_2O $4_{23}-4_{14}$	132.4084	50.6 ± 3.0
$H_2^{17}O$ $4_{23}-4_{14}$	133.0943	11.6 ± 3.1
H_2O $8_{36}-7_{43}$	133.5491	14.8 ± 3.1
H_2O ν_2 $3_{13}-2_{02}$	134.1938	10.0 ± 3.1
H_2O ν_2 $3_{22}-3_{13}$	134.5825	9.6 ± 3.1
$H_2^{17}O$ $5_{14}-5_{05}$	134.7376	9.9 ± 3.1

Table C.2. continued.

Molecules	$\lambda(\mu m)$	F_{line} ($\times 10^{-17}$ W m^{-2})
H_2O $5_{14}-5_{05}$	134.9353	36.7 ± 3.1
H_2O $3_{30}-3_{21}$	136.4960	37.1 ± 3.2
H_2O $7_{35}-8_{08}$	137.6831	8.0 ± 3.3
$H_2^{17}O$ $3_{30}-3_{21}$	138.2514	12.9 ± 3.3
H_2O $3_{13}-2_{02}$	138.5278	45.0 ± 3.3
$H_2^{17}O$ $3_{13}-2_{02}$	139.0864	17.1 ± 3.3
H_2O ν_2 $6_{33}-6_{24}$	140.0581	15.9 ± 3.4
H_2O $4_{13}-3_{22}$	144.5179	31.4 ± 3.6
CO (18-17)	144.7842	18.8 ± 3.6
H_2O $4_{31}-4_{22}$	146.9228	43.5 ± 3.4
H_2O $5_{42}-6_{15}$	148.7904	19.0 ± 3.4
H_2O $9_{54}-8_{63}$	152.2396	3.6 ± 3.6
H_2O ν_2 $2_{21}-2_{12}$	153.2704	18.1 ± 3.7
$H_2^{17}O$ $5_{23}-4_{32}$	153.8758	3.3 ± 3.7
H_2O ν_2 $6_{24}-6_{15}$	154.0193	9.8 ± 3.7
H_2O $3_{22}-3_{13}$	156.1940	63.7 ± 4.2
H_2O $5_{23}-4_{32}$	156.2652	21.5 ± 4.2
$H_2^{17}O$ $3_{22}-3_{13}$	157.2836	11.9 ± 6.4
H_2O $3_{31}-4_{04}$	158.3116	17.4 ± 4.3
H_2O $8_{45}-7_{52}$	159.0506	15.5 ± 4.4
H_2O $6_{34}-7_{07}$	159.4003	17.4 ± 4.4
H_2O $5_{32}-5_{23}$	160.5101	33.0 ± 4.5
OH $^2\Pi_{1/2}$ 3/2-1/2	163.1243	64.9 ± 4.6
OH $^2\Pi_{1/2}$ 3/2-1/2	163.3972	63.6 ± 4.6
NH_3 $3_{21}-2_{20}$	165.5965	2.4 ± 4.0
NH_3 $3_{11}-2_{10}$	165.7288	7.2 ± 4.0
H_2O $7_{34}-7_{25}$	166.8147	31.8 ± 4.1
H_2O $6_{24}-6_{15}$	167.0350	37.3 ± 4.1
H_2O $7_{35}-6_{42}$	169.7388	19.6 ± 4.2
NH_3 $3_{20}-2_{21}$	169.9674	24.3 ± 4.2
NH_3 $3_{10}-2_{11}$	169.9888	24.4 ± 4.2
NH_3 $3_{00}-2_{01}$	169.9962	24.4 ± 4.2
H_2O $6_{33}-6_{24}$	170.1392	29.0 ± 4.3
H_2O ν_2 $2_{12}-1_{01}$	170.9276	15.4 ± 4.3
H_2O $5_{33}-6_{06}$	174.6069	2.6 ± 4.5
H_2O $3_{03}-2_{12}$	174.6259	52.2 ± 4.5
H_2O $4_{32}-5_{05}$	174.9201	22.3 ± 4.5
H_2O $2_{12}-1_{01}$	179.5267	46.8 ± 7.0
$H_2^{17}O$ $2_{12}-1_{01}$	180.3302	32.3 ± 7.0
H_2O $2_{21}-2_{12}$	180.4883	39.0 ± 7.0
$H_2^{17}O$ $2_{21}-2_{12}$	182.0899	15.2 ± 7.2
H_2O $4_{13}-4_{04}$	187.1108	30.0 ± 7.6

Table C.3. Line fluxes calculated from PACS spectra of OH 30.1-0.7.

Molecules	$\lambda(\mu m)$	F_{line} ($\times 10^{-17}$ W m^{-2})
H_2O $4_{22}-3_{13}$	57.6365	10.6 ± 2.9
H_2O $4_{32}-3_{21}$	58.6991	16.8 ± 3.0
H_2O $4_{31}-4_{04}$	61.8086	18.6 ± 3.3
H_2O $6_{60}-6_{51}$	63.9281	18.5 ± 3.5
H_2O $6_{25}-5_{14}$	65.1662	15.4 ± 3.3
H_2O $10_{38}-10_{29}$	65.5763	9.7 ± 3.3
H_2O $7_{16}-6_{25}$	66.0927	11.4 ± 3.4
H_2O $3_{31}-2_{20}$	67.0892	16.3 ± 3.5
H_2O $3_{30}-3_{03}$	67.2690	10.4 ± 3.5
H_2O ν_2 $3_{21}-2_{12}$	70.2871	5.1 ± 3.8
H_2O $8_{27}-8_{18}$	70.7026	16.6 ± 3.9
H_2O $5_{24}-4_{13}$	71.0673	20.0 ± 3.5
H_2O $7_{17}-6_{06}$	71.5397	9.1 ± 3.5
H_2O $7_{07}-6_{16}$	71.9470	16.2 ± 3.6
H_2O $8_{17}-8_{08}$	72.0323	11.5 ± 3.6
H_2O $9_{37}-9_{28}$	73.6129	14.8 ± 3.3
H_2O $10_{47}-10_{38}$	73.9603	7.1 ± 3.8
H_2O $9_{55}-9_{46}$	74.5735	6.4 ± 3.8
H_2O $7_{25}-6_{34}$	74.9450	19.5 ± 3.9
H_2O $3_{21}-2_{12}$	75.3807	13.7 ± 3.4
H_2O $8_{54}-8_{45}$	75.4955	17.5 ± 3.4
H_2O $5_{51}-5_{42}$	75.7814	18.9 ± 3.5
H_2O $6_{52}-6_{43}$	75.8300	39.3 ± 3.5
H_2O $5_{50}-5_{41}$	75.9099	23.7 ± 3.5
H_2O $6_{51}-6_{42}$	76.4220	20.4 ± 3.5
H_2O $7_{52}-7_{43}$	77.7615	21.6 ± 3.7
H_2O $4_{23}-3_{12}$	78.7424	34.2 ± 3.7
H_2O $6_{15}-5_{24}$	78.9285	26.5 ± 3.8
OH $^2\Pi_{1/2}$ 1/2–$^2\Pi_{3/2}$ 3/2	79.1173	32.1 ± 3.8
OH $^2\Pi_{1/2}$ 1/2–$^2\Pi_{3/2}$ 3/2	79.1809	21.4 ± 3.8
H_2O $9_{46}-9_{37}$	80.2223	8.2 ± 4.4
H_2O $8_{53}-8_{44}$	80.5568	17.6 ± 4.5
H_2O $7_{26}-7_{17}$	81.2156	24.5 ± 4.6
H_2O $9_{27}-9_{18}$	81.4054	19.8 ± 4.6
H_2O $8_{35}-7_{44}$	81.6902	10.4 ± 4.6
H_2O $6_{16}-5_{05}$	82.0315	24.9 ± 4.7
H_2O $8_{36}-8_{27}$	82.9767	27.6 ± 4.8
H_2O $6_{06}-5_{15}$	83.2840	22.0 ± 4.8
H_2O $7_{16}-7_{07}$	84.7670	25.1 ± 5.0
H_2O $9_{54}-9_{45}$	85.4248	13.5 ± 3.8
H_2O $8_{45}-8_{36}$	85.7688	25.9 ± 3.8
H_2O $3_{22}-2_{11}$	89.9884	33.3 ± 4.2
H_2O $7_{44}-7_{35}$	90.0498	27.2 ± 4.2
$H_2^{17}O$ $3_{22}-2_{11}$	90.4885	7.9 ± 4.2
H_2O $6_{43}-6_{34}$	92.8108	42.5 ± 4.5
H_2O $7_{35}-7_{26}$	93.3829	32.4 ± 4.5
H_2O $5_{42}-5_{33}$	94.2096	32.8 ± 4.6
H_2O $6_{25}-6_{16}$	94.6441	34.2 ± 4.6
H_2O $4_{41}-4_{32}$	94.7052	44.1 ± 4.6
H_2O $6_{15}-6_{06}$	103.9402	22.8 ± 2.8
H_2O $6_{34}-6_{25}$	104.0937	18.2 ± 1.9
H_2S $6_{43}-5_{32}$	104.5727	2.6 ± 1.9
$H_2^{17}O$ $6_{34}-6_{25}$	104.7528	2.9 ± 1.9
H_2O $2_{21}-1_{10}$	108.0732	9.6 ± 2.0
$H_2^{17}O$ $2_{21}-1_{10}$	108.7449	3.1 ± 2.0
H_2O $5_{24}-5_{15}$	111.6280	14.8 ± 1.6
H_2O $7_{43}-7_{34}$	112.5106	11.6 ± 1.6
H_2O $4_{41}-5_{14}$	112.8029	2.7 ± 1.6
H_2O $4_{14}-3_{03}$	113.5374	13.8 ± 1.7
H_2O $5_{33}-5_{24}$	113.9480	22.8 ± 1.7
H_2O $7_{34}-6_{43}$	116.7791	5.1 ± 1.8
OH $^2\Pi_{3/2}$ 5/2-3/2	119.2342	−4.9 ± 1.8
OH $^2\Pi_{3/2}$ 5/2-3/2	119.4417	−5.0 ± 1.8
H_2O $4_{32}-4_{23}$	121.7217	25.4 ± 1.3

Notes. [(a)] The line is blended with a nearby transition.

Table C.3. continued.

Molecules	$\lambda(\mu m)$	F_{line} ($\times 10^{-17}$ W m^{-2})
H_2O $8_{44}-8_{35}$	122.5222	5.6 ± 1.3
$H_2^{17}O$ $4_{32}-4_{23}$	122.8999	4.3 ± 1.3
H_2O $9_{36}-9_{27}$	123.4605	4.3 ± 1.3
H_2O $4_{04}-3_{13}$	125.3537	12.2 ± 1.4
H_2O $3_{31}-3_{22}$	126.7140	16.1 ± 1.4
NH_3 $4_{10}-3_{11}$	127.1811	2.4 ± 1.4
H_2O $7_{25}-7_{16}$	127.8842	12.0 ± 1.4
H_2O $9_{45}-9_{36}$	129.3390	5.6 ± 1.4
H_2O $4_{23}-4_{14}$	132.4084	17.8 ± 1.2
$H_2^{17}O$ $4_{23}-4_{14}$	133.0943	3.3 ± 1.2
H_2O $8_{36}-7_{43}$	133.5491	3.6 ± 1.2
H_2O $5_{14}-5_{05}$	134.9353	13.2 ± 1.2
H_2O $3_{30}-3_{21}$	136.4960	12.5 ± 1.2
H_2O $3_{13}-2_{02}$	138.5278	13.8 ± 1.3
$H_2^{17}O$ $3_{13}-2_{02}$	139.0864	3.9 ± 1.3
H_2O $4_{13}-3_{22}$	144.5179	10.0 ± 1.4
H_2S^a $3_{21}-2_{12}$	144.7797	5.4 ± 1.4
CO^a (18−17)	144.7842	5.4 ± 1.4
H_2O $4_{31}-4_{22}$	146.9228	14.8 ± 1.5
H_2O $5_{42}-6_{15}$	148.7904	4.6 ± 1.5
H_2S $4_{32}-3_{21}$	150.1524	4.6 ± 1.2
H_2O^a $3_{22}-3_{13}$	156.1940	20.9 ± 1.3
H_2O^a $5_{23}-4_{32}$	156.2652	2.1 ± 1.3
$H_2^{17}O$ $3_{22}-3_{13}$	157.2836	1.8 ± 1.3
H_2O $3_{31}-4_{04}$	158.3116	3.3 ± 1.3
H_2O $6_{34}-7_{07}$	159.4003	3.0 ± 1.3
H_2O $5_{32}-5_{23}$	160.5101	11.4 ± 1.3
H_2S $5_{14}-4_{23}$	161.8151	2.7 ± 1.4
H_2S^a $6_{06}-5_{15}$	162.3344	3.5 ± 1.4
H_2S^a $6_{16}-5_{05}$	162.3344	3.5 ± 1.4
OH $^2\Pi_{1/2}$ 3/2−1/2	163.1243	15.9 ± 1.4
OH $^2\Pi_{1/2}$ 3/2−1/2	163.3972	15.4 ± 1.4
H_2O $7_{34}-7_{25}$	166.8147	8.1 ± 1.4
H_2O $6_{24}-6_{15}$	167.0350	11.2 ± 1.4
H_2O $6_{33}-6_{24}$	170.1392	7.5 ± 1.5
H_2O^a $5_{33}-6_{06}$	174.6069	2.6 ± 1.6
H_2O^a $3_{03}-2_{12}$	174.6259	17.4 ± 1.6
H_2O $4_{32}-5_{05}$	174.9201	6.9 ± 1.6
H_2S $3_{31}-2_{20}$	175.5257	3.8 ± 1.6
H_2O $2_{12}-1_{01}$	179.5267	10.7 ± 1.7
H_2O $2_{21}-2_{12}$	180.4883	11.2 ± 1.7
H_2O $4_{13}-4_{04}$	187.1108	10.9 ± 1.8

Table C.4. Line fluxes calculated from PACS spectra of OH 32.0-0.5.

Molecules	$\lambda(\mu m)$	F_{line} ($\times 10^{-17}$ W m^{-2})
H_2O $6_{60}-6_{51}$	63.9281	10.3 ± 28.2
H_2O $6_{25}-5_{14}$	65.1662	4.8 ± 2.9
H_2O $3_{30}-2_{21}$	66.4377	4.3 ± 3.1
H_2O $3_{31}-2_{20}$	67.0892	5.7 ± 1.9
H_2O $3_{30}-3_{03}$	67.2690	7.7 ± 2.0
H_2O ν_2 $3_{21}-2_{12}$	70.2871	3.5 ± 2.1
H_2O $8_{27}-8_{18}$	70.7026	6.6 ± 2.6
H_2O $5_{24}-4_{13}$	71.0673	5.7 ± 2.6
H_2O $7_{17}-6_{06}$	71.5397	3.7 ± 2.7
H_2O $7_{07}-6_{16}$	71.9470	4.8 ± 2.7
H_2O $8_{17}-8_{08}$	72.0323	3.3 ± 2.7
H_2O $9_{37}-9_{28}$	73.6129	6.3 ± 1.9
H_2O ν_2 $4_{23}-3_{12}$	73.7448	5.3 ± 1.9
H_2O $10_{47}-10_{38}$	73.9603	3.8 ± 1.9
H_2O $7_{25}-6_{34}$	74.9450	8.0 ± 1.9
H_2O $3_{21}-2_{12}$	75.3807	3.9 ± 2.2
H_2O $8_{54}-8_{45}$	75.4955	6.3 ± 2.2
$H_2^{17}O$ $3_{21}-2_{12}$	75.6381	3.4 ± 2.2
H_2O^a $5_{51}-5_{42}$	75.7814	7.4 ± 1.8
H_2O^a $6_{52}-6_{43}$	75.8300	14.4 ± 1.7
H_2O $5_{50}-5_{41}$	75.9099	8.6 ± 1.7
H_2O $6_{51}-6_{42}$	76.4220	7.4 ± 1.8
H_2O $7_{52}-7_{43}$	77.7615	7.5 ± 1.8
H_2O $4_{23}-3_{12}$	78.7424	12.5 ± 1.9
H_2O ν_2 $6_{43}-6_{34}$	78.9458	8.0 ± 1.9
OH $^2\Pi_{1/2}$ 1/2–$^2\Pi_{3/2}$ 3/2	79.1173	12.0 ± 1.9
OH $^2\Pi_{1/2}$ 1/2–$^2\Pi_{3/2}$ 3/2	79.1809	8.5 ± 1.9
H_2O $9_{46}-9_{37}$	80.2223	5.6 ± 1.7
H_2O $8_{53}-8_{44}$	80.5568	4.0 ± 1.7
H_2O $7_{26}-7_{17}$	81.2156	7.1 ± 1.7
H_2O $9_{27}-9_{18}$	81.4054	6.7 ± 1.7
H_2O $8_{35}-7_{44}$	81.6902	4.3 ± 1.7
H_2O $6_{16}-5_{05}$	82.0315	5.9 ± 1.7
H_2O $8_{36}-8_{27}$	82.9767	7.5 ± 1.8
H_2O $6_{06}-5_{15}$	83.2840	8.0 ± 1.8
H_2O $7_{16}-7_{07}$	84.7670	11.3 ± 1.9
H_2O $9_{54}-9_{45}$	85.4248	4.2 ± 1.9
H_2O $8_{45}-8_{36}$	85.7688	7.4 ± 1.9
H_2O $3_{22}-2_{11}$	89.9884	12.4 ± 2.1
H_2O $7_{44}-7_{35}$	90.0498	10.9 ± 2.8
$H_2^{17}O$ $3_{22}-2_{11}$	90.4885	2.5 ± 2.8
H_2O ν_2 $2_{20}-1_{11}$	92.1496	4.6 ± 2.9
H_2O $6_{43}-6_{34}$	92.8108	11.6 ± 3.0
H_2O $7_{35}-7_{26}$	93.3829	7.4 ± 3.0
H_2O $5_{42}-5_{33}$	94.2096	11.6 ± 3.1
H_2O $6_{25}-6_{16}$	94.6441	11.0 ± 3.1
H_2O $4_{41}-4_{32}$	94.7052	9.6 ± 3.1
H_2O ν_2 $5_{15}-4_{04}$	94.8966	3.7 ± 3.1
H_2O $6_{15}-6_{06}$	103.9402	7.6 ± 1.1
H_2O $6_{34}-6_{25}$	104.0937	5.9 ± 1.1
H_2O $2_{21}-1_{10}$	108.0732	3.7 ± 1.0
$H_2^{17}O$ $2_{21}-1_{10}$	108.7449	2.8 ± 1.0
H_2O $5_{24}-5_{15}$	111.6280	4.6 ± 1.1
H_2O $7_{43}-7_{34}$	112.5106	3.9 ± 1.1
H_2O $4_{14}-3_{03}$	113.5374	5.1 ± 1.1
H_2O $5_{33}-5_{24}$	113.9480	5.5 ± 1.1
H_2O $7_{34}-6_{43}$	116.7791	2.4 ± 1.5
OH $^2\Pi_{3/2}$ 5/2-3/2	119.2342	-3.2 ± 1.2
OH $^2\Pi_{3/2}$ 5/2-3/2	119.4417	-2.0 ± 1.2
H_2O $4_{32}-4_{23}$	121.7217	7.7 ± 1.3
H_2O $8_{44}-8_{35}$	122.5222	2.8 ± 1.3
$H_2^{17}O$ $4_{32}-4_{23}$	122.8999	2.1 ± 1.3
H_2O $9_{36}-9_{27}$	123.4605	2.4 ± 1.3
H_2O ν_2 $5_{14}-5_{05}$	124.8494	1.5 ± 1.3

Notes. [a] The line is blended with a nearby transition.

Table C.4. continued.

Molecules	$\lambda(\mu m)$	F_{line} ($\times 10^{-17}$ W m^{-2})
NH_3 $4_{01}-3_{00}$	124.9125	1.6 ± 1.3
H_2O $4_{04}-3_{13}$	125.3537	4.9 ± 1.4
H_2O $3_{31}-3_{22}$	126.7140	5.4 ± 1.4
NH_3 $4_{10}-3_{11}$	127.1811	1.6 ± 1.4
H_2O $7_{25}-7_{16}$	127.8842	4.5 ± 1.4
H_2O $9_{45}-9_{36}$	129.3390	1.8 ± 1.4
H_2O $4_{23}-4_{14}$	132.4084	8.3 ± 1.1
$H_2^{17}O$ $4_{23}-4_{14}$	133.0943	1.6 ± 1.1
H_2O $8_{36}-7_{43}$	133.5491	3.1 ± 1.1
H_2O ν_2 $3_{13}-2_{02}$	134.1938	1.5 ± 1.1
H_2O $5_{14}-5_{05}$	134.9353	5.4 ± 1.1
H_2O $3_{30}-3_{21}$	136.4960	5.8 ± 1.1
H_2O $3_{13}-2_{02}$	138.5278	6.0 ± 1.2
$H_2^{17}O$ $3_{13}-2_{02}$	139.0864	2.8 ± 1.2
H_2O $4_{13}-3_{22}$	144.5179	4.7 ± 1.3
H_2O $4_{31}-4_{22}$	146.9228	4.0 ± 1.3
H_2O $5_{42}-6_{15}$	148.7904	1.9 ± 1.3
H_2O ν_2 $2_{21}-2_{12}$	153.2704	1.9 ± 1.4
H_2O^a $3_{22}-3_{13}$	156.1940	10.3 ± 1.5
H_2O^a $5_{23}-4_{32}$	156.2652	3.5 ± 1.5
H_2O $3_{31}-4_{04}$	158.3116	10.6 ± 1.5
H_2O $5_{32}-5_{23}$	160.5101	5.0 ± 1.6
OH $^2\Pi_{1/2}$ 3/2-1/2	163.1243	6.8 ± 1.8
OH $^2\Pi_{1/2}$ 3/2-1/2	163.3972	7.5 ± 1.8
H_2O $7_{34}-7_{25}$	166.8147	6.0 ± 1.9
H_2O $6_{24}-6_{15}$	167.0350	6.2 ± 1.9
H_2O $7_{35}-6_{42}$	169.7388	2.7 ± 2.0
H_2O $6_{33}-6_{24}$	170.1392	3.6 ± 1.8
H_2O ν_2 $2_{12}-1_{01}$	170.9276	2.7 ± 1.8
H_2O $5_{33}-6_{06}$	174.6069	7.5 ± 1.8
H_2O $2_{12}-1_{01}$	179.5267	5.9 ± 2.2
H_2O $2_{21}-2_{12}$	180.4883	4.4 ± 2.5
H_2O $4_{13}-4_{04}$	187.1108	6.7 ± 3.0

Table C.5. Line fluxes calculated from PACS spectra of OH 32.8-0.3.

Molecules	$\lambda(\mu m)$	F_{line} ($\times 10^{-17}$ W m^{-2})
H_2O $4_{32}-3_{21}$	58.6991	17.4 ± 3.9
H_2O $7_{26}-6_{15}$	59.9871	9.6 ± 4.0
H_2O $8_{26}-7_{35}$	60.1622	9.1 ± 4.1
H_2O $4_{31}-4_{04}$	61.8086	15.2 ± 4.3
H_2O $9_{28}-9_{19}$	62.4316	8.8 ± 4.4
H_2O $8_{18}-7_{07}$	63.3236	6.7 ± 4.5
H_2O $8_{08}-7_{17}$	63.4580	7.5 ± 4.5
H_2O $6_{60}-6_{51}$	63.9281	26.0 ± 4.6
H_2O $9_{64}-9_{55}$	63.9940	11.5 ± 4.6
H_2O $8_{62}-8_{53}$	64.2136	8.6 ± 4.6
H_2O $6_{25}-5_{14}$	65.1662	16.4 ± 4.0
H_2S $6_{61}-5_{32}$	65.4293	7.0 ± 4.1
H_2O $10_{38}-10_{29}$	65.5763	9.9 ± 4.1
H_2O $7_{16}-6_{25}$	66.0927	14.5 ± 4.2
H_2O $10_{64}-10_{55}$	66.3322	7.2 ± 4.2
H_2O $3_{30}-2_{21}$	66.4377	10.7 ± 4.2
H_2O $3_{31}-2_{20}$	67.0892	19.0 ± 4.3
H_2O $3_{30}-3_{03}$	67.2690	12.7 ± 4.3
H_2O ν_2 $3_{21}-2_{12}$	70.2871	8.5 ± 0.5
H_2O $8_{27}-8_{18}$	70.7026	15.4 ± 3.5
H_2O $5_{24}-4_{13}$	71.0673	16.5 ± 3.5
H_2O $7_{17}-6_{06}$	71.5397	10.4 ± 3.5
H_2O $7_{07}-6_{16}$	71.9470	11.7 ± 3.6
H_2O ν_2 $7_{07}-6_{16}$	72.5218	11.0 ± 3.6
H_2O $10_{56}-10_{47}$	72.7893	9.3 ± 3.7
H_2O $9_{37}-9_{28}$	73.6129	14.2 ± 3.3
H_2O ν_2 $4_{23}-3_{12}$	73.7448	9.0 ± 3.3
H_2O $10_{47}-10_{38}$	73.9603	7.8 ± 3.3
H_2O $7_{25}-6_{34}$	74.9450	16.8 ± 3.4
H_2O $3_{21}-2_{12}$	75.3807	8.2 ± 3.4
H_2O $8_{54}-8_{45}$	75.4955	13.8 ± 3.4
H_2O $5_{51}-5_{42}$	75.7814	15.8 ± 3.5
H_2O $6_{52}-6_{43}$	75.8300	35.9 ± 3.5
H_2O $5_{50}-5_{41}$	75.9099	20.9 ± 3.5
H_2O $6_{51}-6_{42}$	76.4220	13.9 ± 3.5
H_2O $7_{52}-7_{43}$	77.7615	16.2 ± 3.7
H_2O $4_{23}-3_{12}$	78.7424	27.9 ± 3.7
H_2O $6_{15}-5_{24}$	78.9285	25.4 ± 3.8
OH $^2\Pi_{1/2}$ 1/2–$^2\Pi_{3/2}$ 3/2	79.1173	27.4 ± 3.8
OH $^2\Pi_{1/2}$ 1/2–$^2\Pi_{3/2}$ 3/2	79.1809	27.4 ± 3.8
H_2O $9_{46}-9_{37}$	80.2223	10.0 ± 4.4
H_2O $8_{53}-8_{44}$	80.5568	12.4 ± 4.5
H_2O $7_{26}-7_{17}$	81.2156	17.8 ± 4.6
H_2O $9_{27}-9_{18}$	81.4054	15.0 ± 4.6
H_2O $11_{38}-11_{29}$	81.5934	7.8 ± 4.6
H_2O $8_{35}-7_{44}$	81.6902	10.3 ± 4.6
H_2O $6_{16}-5_{05}$	82.0315	19.4 ± 4.7
H_2O $8_{36}-8_{27}$	82.9767	22.2 ± 4.8
H_2O $6_{06}-5_{15}$	83.2840	20.1 ± 4.8
H_2O $7_{16}-7_{07}$	84.7670	26.8 ± 5.0
H_2O $9_{54}-9_{45}$	85.4248	15.3 ± 4.1
H_2O $8_{45}-8_{36}$	85.7688	24.0 ± 4.1
H_2O $3_{22}-2_{11}$	89.9884	22.5 ± 4.2
H_2O $7_{44}-7_{35}$	90.0498	23.9 ± 3.5
H_2O ν_2 $2_{20}-1_{11}$	92.1496	12.5 ± 3.7
H_2O $6_{43}-6_{34}$	92.8108	35.1 ± 3.7
H_2O $7_{35}-7_{26}$	93.3829	23.6 ± 3.8
H_2O $5_{42}-5_{33}$	94.2096	29.3 ± 3.8
H_2O $6_{25}-6_{16}$	94.6441	31.0 ± 3.9
H_2O $4_{41}-4_{32}$	94.7052	28.0 ± 3.9
H_2O $6_{15}-6_{06}$	103.9402	16.7 ± 1.8
H_2O $6_{34}-6_{25}$	104.0937	14.5 ± 1.8
$H_2^{17}O$ $6_{34}-6_{25}$	104.7528	4.8 ± 1.8
H_2O $2_{21}-1_{10}$	108.0732	6.5 ± 1.9

Notes. [(a)] The line is blended with a nearby transition.

Table C.5. continued.

Molecules	$\lambda(\mu m)$	F_{line} ($\times 10^{-17}$ W m^{-2})
$H_2^{17}O$ $2_{21}-1_{10}$	108.7449	4.0 ± 1.9
H_2O ν_2 $4_{14}-3_{03}$	111.4826	3.1 ± 1.8
H_2O $5_{24}-5_{15}$	111.6280	9.6 ± 1.8
H_2O $7_{43}-7_{34}$	112.5106	7.7 ± 1.9
H_2O $4_{41}-5_{14}$	112.8029	3.1 ± 1.9
H_2O ν_2 $3_{30}-3_{21}$	113.2751	2.7 ± 1.9
H_2O $4_{14}-3_{03}$	113.5374	12.5 ± 1.9
H_2O $5_{33}-5_{24}$	113.9480	16.9 ± 1.9
H_2O $9_{27}-10_{1*}$	114.4537	3.0 ± 1.9
H_2O $10_{38}-9_{45}$	116.4241	3.0 ± 2.0
H_2O $7_{34}-6_{43}$	116.7791	3.9 ± 2.0
H_2O $4_{32}-4_{23}$	121.7217	17.2 ± 1.3
H_2S $6_{34}-5_{23}$	122.2450	2.0 ± 1.3
H_2O $8_{44}-8_{35}$	122.5222	5.0 ± 1.3
$H_2^{17}O$ $4_{32}-4_{23}$	122.8999	2.5 ± 1.3
H_2O $9_{36}-9_{27}$	123.4605	4.4 ± 1.3
H_2S^a $7_{26}-6_{15}$	123.8264	1.3 ± 1.3
H_2S^a $7_{16}-6_{25}$	123.8401	2.1 ± 1.3
H_2O ν_2 $5_{14}-5_{05}$	124.8494	2.0 ± 1.3
H_2O $4_{04}-3_{13}$	125.3537	9.4 ± 1.4
H_2O $3_{31}-3_{22}$	126.7140	13.9 ± 1.4
H_2O $7_{25}-7_{16}$	127.8842	8.8 ± 1.4
H_2O ν_2 $4_{04}-3_{13}$	128.2586	3.0 ± 1.4
H_2O $9_{45}-9_{36}$	129.3390	4.4 ± 1.4
H_2O $4_{23}-4_{14}$	132.4084	13.2 ± 1.2
$H_2^{17}O$ $4_{23}-4_{14}$	133.0943	2.3 ± 1.2
H_2O $8_{36}-7_{43}$	133.5491	2.7 ± 1.2
H_2O ν_2 $3_{13}-2_{02}$	134.1938	2.8 ± 1.2
H_2O ν_2 $3_{22}-3_{13}$	134.5825	2.5 ± 1.3
$H_2^{17}O$ $5_{14}-5_{05}$	134.7376	2.3 ± 1.3
H_2O $5_{14}-5_{05}$	134.9353	9.4 ± 12.6
H_2O $3_{30}-3_{21}$	136.4960	9.1 ± 12.9
H_2O $3_{13}-2_{02}$	138.5278	9.7 ± 1.3
$H_2^{17}O$ $3_{13}-2_{02}$	139.0864	3.0 ± 1.3
H_2O $4_{13}-3_{22}$	144.5179	6.2 ± 1.4
CO (18–17)	144.7842	2.3 ± 1.4
H_2O $4_{31}-4_{22}$	146.9228	10.3 ± 1.5
H_2O $5_{42}-6_{15}$	148.7904	4.7 ± 1.5
H_2O ν_2 $2_{21}-2_{12}$	153.2704	2.1 ± 1.6
H_2O $3_{22}-3_{13}$	156.1940	13.8 ± 1.7
H_2O $3_{31}-4_{04}$	158.3116	3.3 ± 1.7
H_2O $5_{32}-5_{23}$	160.5101	7.1 ± 1.1
OH $^2\Pi_{1/2}$ 3/2-1/2	163.1243	10.0 ± 1.1
OH $^2\Pi_{1/2}$ 3/2-1/2	163.3972	8.9 ± 1.2
H_2O $7_{34}-7_{25}$	166.8147	3.3 ± 1.2
H_2O $6_{24}-6_{15}$	167.0350	5.2 ± 1.2
H_2O $6_{33}-6_{24}$	170.1392	3.1 ± 0.8
H_2O^a $5_{33}-6_{06}$	174.6069	1.8 ± 0.8
H_2O^a $3_{03}-2_{12}$	174.6259	5.4 ± 0.8
H_2O $4_{32}-5_{05}$	174.9201	2.7 ± 0.8
H_2S $3_{31}-2_{20}$	175.5257	1.0 ± 0.8
H_2O $2_{12}-1_{01}$	179.5267	2.4 ± 0.8
$H_2^{17}O$ $2_{12}-1_{01}$	180.3302	0.7 ± 0.7
H_2O $2_{21}-2_{12}$	180.4883	1.3 ± 0.7
H_2O $4_{13}-4_{04}$	187.1108	1.5 ± 0.8

Table C.6. Line fluxes calculated from PACS spectra of OH 42.3-0.1.

Molecules	$\lambda(\mu m)$	F_{line} ($\times 10^{-17}$ W m^{-2})
H_2O $6_{25}-5_{14}$	65.1662	3.1 ± 1.7
H_2O $3_{30}-2_{21}$	66.4377	3.1 ± 1.7
H_2O $3_{31}-2_{20}$	67.0892	4.6 ± 1.7
H_2O $3_{30}-3_{03}$	67.2690	6.9 ± 1.8
H_2O $7_{07}-6_{16}$	71.9470	7.9 ± 3.8
H_2O $9_{37}-9_{28}$	73.6129	5.7 ± 2.8
H_2O ν_2 $4_{23}-3_{12}$	73.7448	6.4 ± 2.8
H_2O $10_{47}-10_{38}$	73.9603	4.9 ± 2.8
H_2O $9_{55}-9_{46}$	74.5735	4.7 ± 2.9
H_2O $7_{25}-6_{34}$	74.9450	7.4 ± 2.9
H_2O $3_{21}-2_{12}$	75.3807	7.3 ± 2.9
H_2O $8_{54}-8_{45}$	75.4955	3.8 ± 3.0
H_2O^a $5_{51}-5_{42}$	75.7814	4.2 ± 3.0
H_2O^a $7_{53}-7_{44}$	75.8134	8.0 ± 3.0
H_2O^a $6_{52}-6_{43}$	75.8300	4.7 ± 3.0
H_2O $5_{50}-5_{41}$	75.9099	7.7 ± 3.0
H_2O $6_{51}-6_{42}$	76.4220	4.3 ± 3.0
H_2O $7_{52}-7_{43}$	77.7615	7.1 ± 3.1
H_2O $4_{23}-3_{12}$	78.7424	8.2 ± 3.2
H_2O $9_{27}-9_{18}$	81.4054	6.6 ± 3.4
H_2O $6_{16}-5_{05}$	82.0315	7.4 ± 3.5
H_2O ν_2 $5_{41}-5_{32}$	82.3939	4.4 ± 3.5
H_2O $8_{36}-8_{27}$	82.9767	8.4 ± 3.6
H_2O $6_{06}-5_{15}$	83.2840	6.5 ± 3.6
H_2O $7_{16}-7_{07}$	84.7670	6.7 ± 3.7
H_2O $8_{45}-8_{36}$	85.7688	7.3 ± 3.8
H_2O $3_{22}-2_{11}$	89.9884	12.9 ± 4.2
H_2O $7_{44}-7_{35}$	90.0498	7.9 ± 3.6
H_2O $6_{43}-6_{34}$	92.8108	15.0 ± 3.9
H_2O $5_{42}-5_{33}$	94.2096	9.2 ± 4.1
H_2O $6_{25}-6_{16}$	94.6441	12.3 ± 4.1
H_2O $4_{41}-4_{32}$	94.7052	9.7 ± 4.1
H_2O^a $6_{42}-6_{33}$	103.9163	5.6 ± 1.3
H_2O^a $6_{15}-6_{06}$	103.9402	5.6 ± 1.3
H_2O $6_{34}-6_{25}$	104.0937	4.3 ± 0.9
H_2O $2_{21}-1_{10}$	108.0732	2.0 ± 1.4
H_2O $5_{24}-5_{15}$	111.6280	5.6 ± 1.3
H_2O $7_{43}-7_{34}$	112.5106	2.3 ± 1.3
H_2O $4_{14}-3_{03}$	113.5374	4.5 ± 1.3
H_2O $5_{33}-5_{24}$	113.9480	4.4 ± 1.3
OH $^2\Pi_{3/2}$ 5/2-3/2	119.2342	−3.2 ± 1.5
OH $^2\Pi_{3/2}$ 5/2-3/2	119.4417	−1.7 ± 1.5
H_2O $4_{32}-4_{23}$	121.7217	7.0 ± 1.3
H_2O $4_{04}-3_{13}$	125.3537	3.9 ± 1.4
H_2O $3_{31}-3_{22}$	126.7140	3.4 ± 1.4
H_2O $7_{25}-7_{16}$	127.8842	1.9 ± 1.4
H_2O $4_{23}-4_{14}$	132.4084	3.5 ± 0.8
H_2O $8_{36}-7_{43}$	133.5491	2.6 ± 0.8
H_2O $5_{14}-5_{05}$	134.9353	3.4 ± 0.8
H_2O $3_{30}-3_{21}$	136.4960	3.0 ± 0.8
$H_2^{17}O$ $3_{30}-3_{21}$	138.2514	1.7 ± 0.8
H_2O $3_{13}-2_{02}$	138.5278	3.5 ± 0.8
H_2O $4_{13}-3_{22}$	144.5179	3.1 ± 0.9
H_2O $4_{31}-4_{22}$	146.9228	3.5 ± 0.9
H_2O ν_2 $2_{21}-2_{12}$	153.2704	2.2 ± 1.1
H_2O^a $3_{22}-3_{13}$	156.1940	5.0 ± 1.2
H_2O^a $5_{23}-4_{32}$	156.2652	0.9 ± 1.2

Notes. [a] The line is blended with a nearby transition.

Table C.6. continued.

Molecules	$\lambda(\mu m)$	F_{line} ($\times 10^{-17}$ W m^{-2})
H_2O $5_{32}-5_{23}$	160.5101	3.7 ± 0.7
OH $^2\Pi_{1/2}$ 3/2−1/2	163.1243	1.8 ± 0.7
OH $^2\Pi_{1/2}$ 3/2−1/2	163.3972	2.8 ± 0.7
H_2O $7_{34}-7_{25}$	166.8147	2.1 ± 0.7
H_2O $6_{24}-6_{15}$	167.0350	1.7 ± 0.7
H_2O $6_{33}-6_{24}$	170.1392	1.8 ± 0.8
H_2O^a $5_{33}-6_{06}$	174.6069	1.6 ± 0.8
H_2O^a $3_{03}-2_{12}$	174.6259	2.4 ± 0.8
H_2O $4_{32}-5_{05}$	174.9201	1.3 ± 0.8
$H_2^{17}O$ $2_{12}-1_{01}$	180.3302	3.3 ± 1.0
H_2O $4_{13}-4_{04}$	187.1108	3.8 ± 1.1

Appendix D: SPIRE spectra

This section shows the continuum subtracted apodized SPIRE spectra (in W m^{-2} μm^{-1}) of the stars in our sample (histogram) together with the Gaussian fits for H_2O (red), $H_2^{17}O$ (blue), CO (green) and H_2S (yellow). Other molecules are shown in cyan.

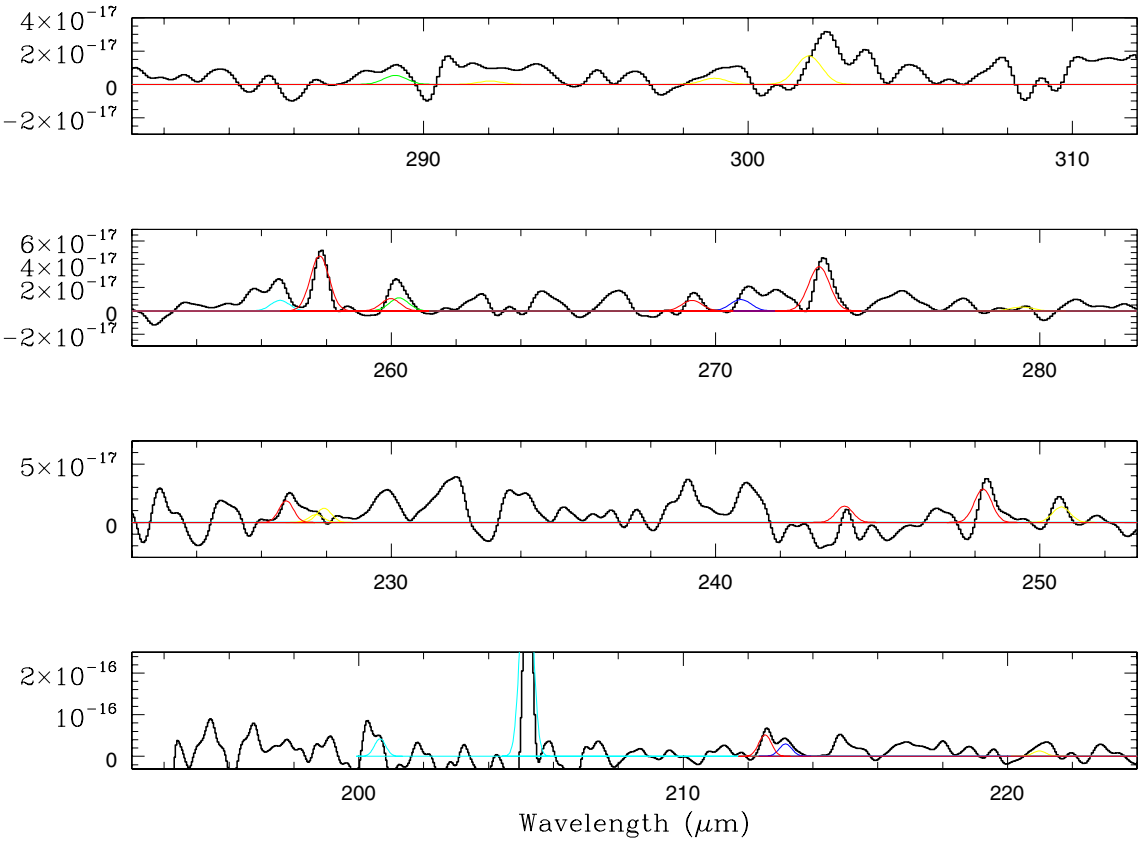

Fig. D.1. The continuum subtracted apodized SPIRE spectrum of OH21.5+0.5.

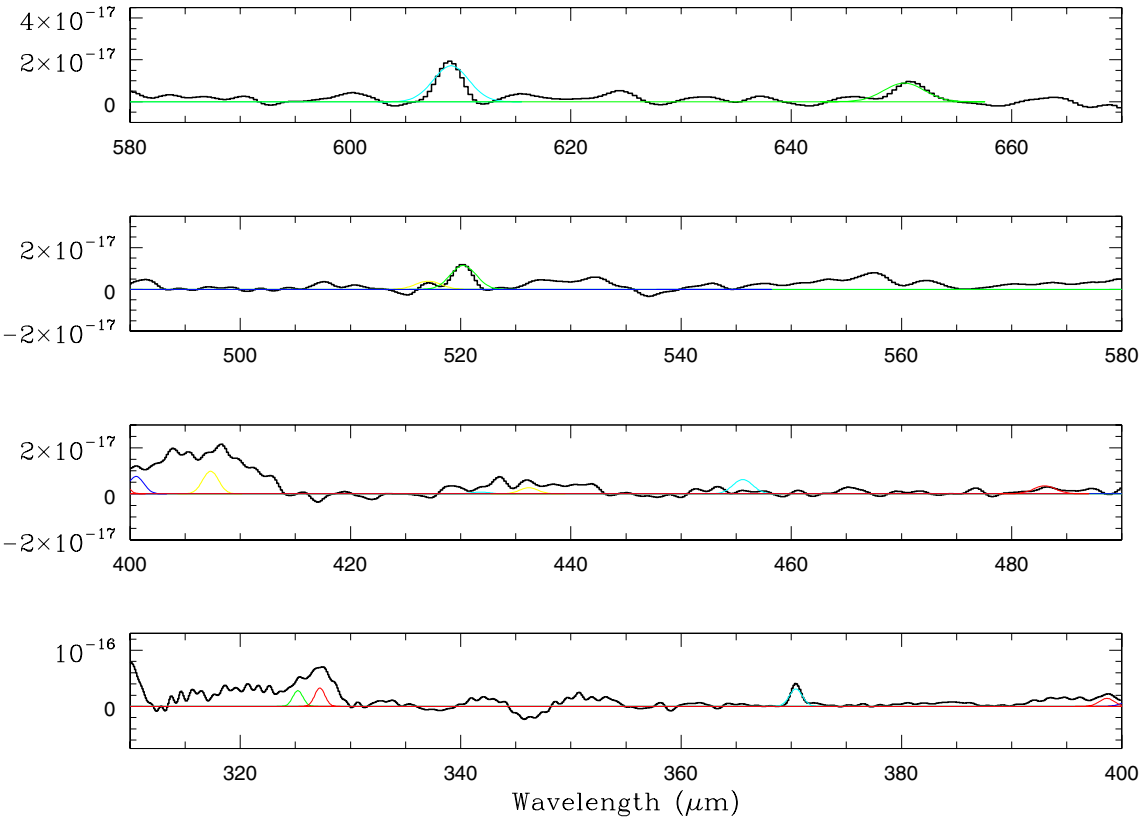

Fig. D.2. The continuum subtracted apodized SPIRE spectrum of OH21.5+0.5.

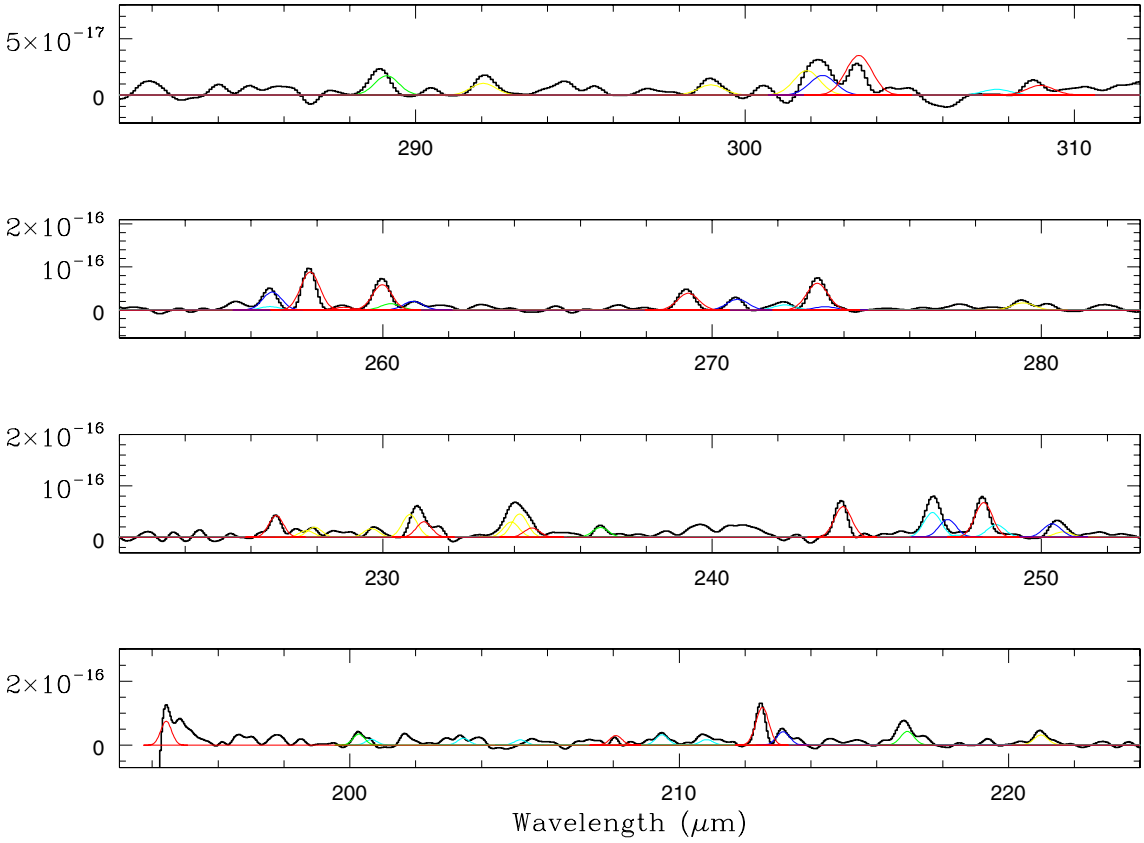

Fig. D.3. The continuum subtracted apodized SPIRE spectrum of OH 127.8+0.0.

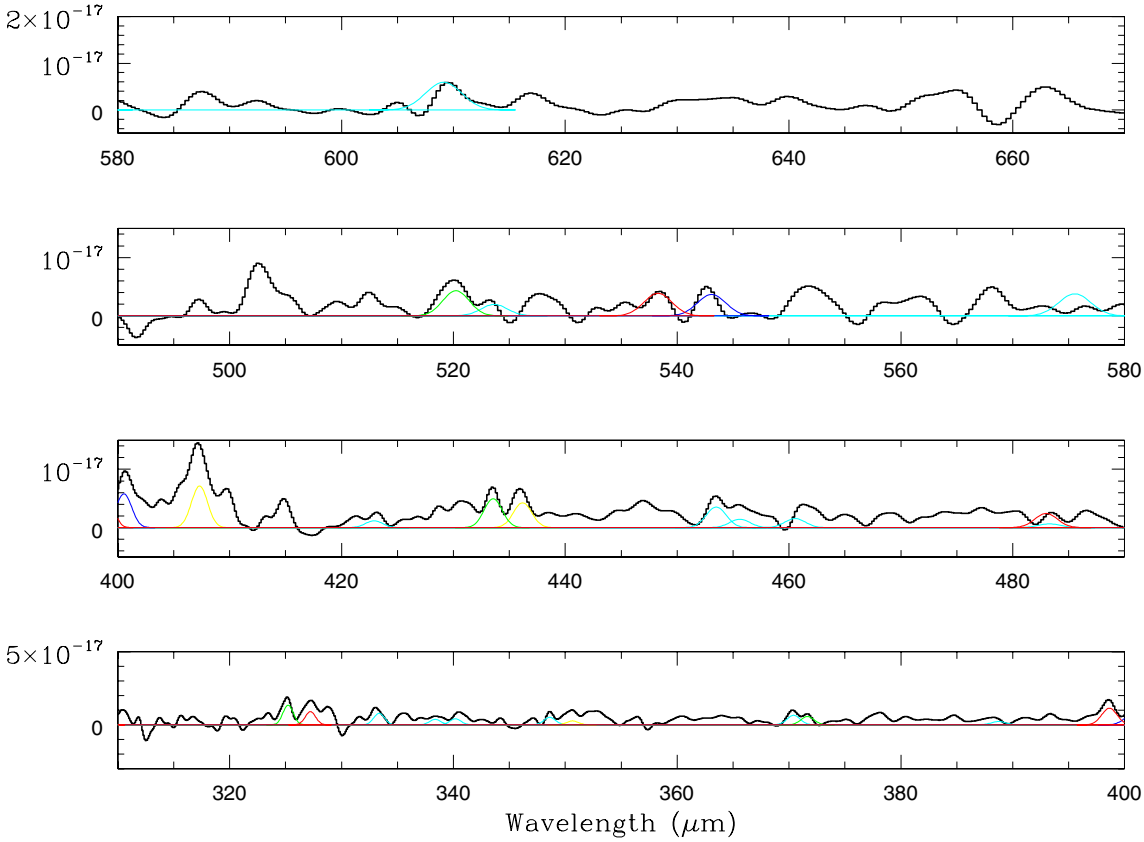

Fig. D.4. The continuum subtracted apodized SPIRE spectrum of OH 127.8+0.0.

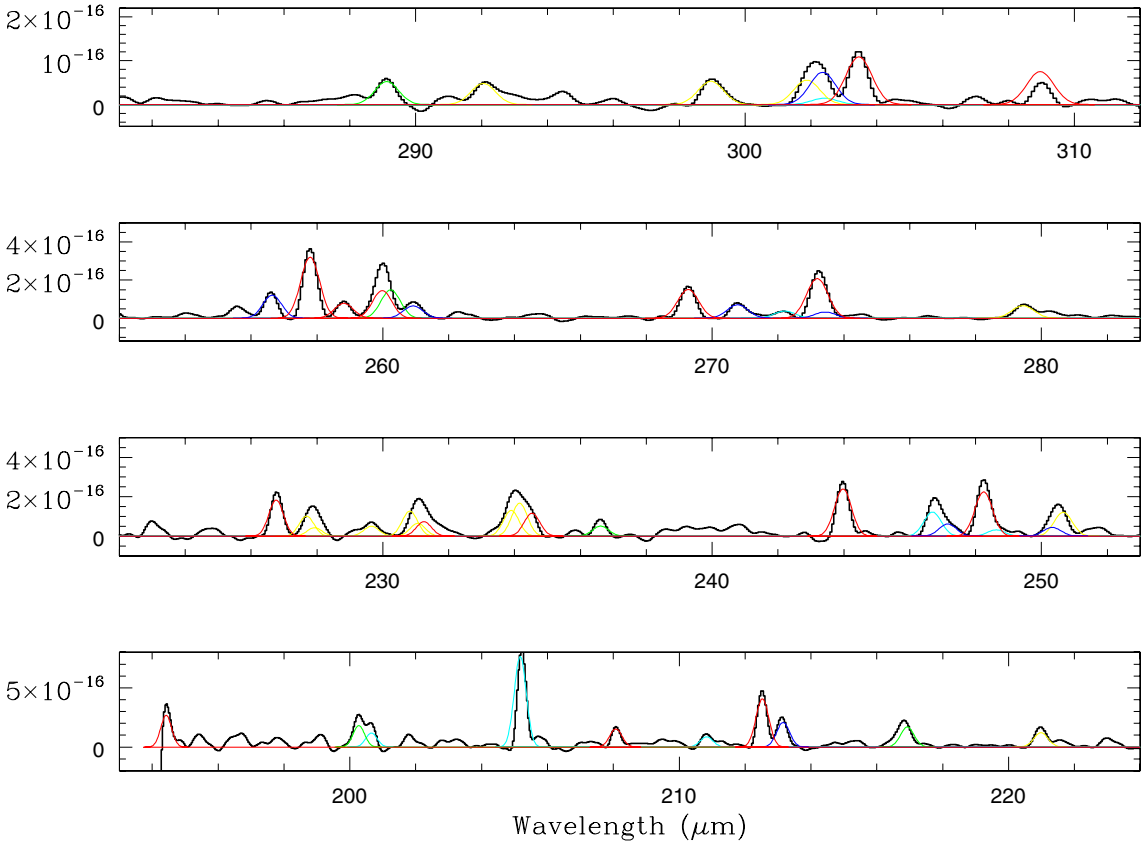

Fig. D.5. The continuum subtracted apodized SPIRE spectrum of OH 26.5+0.6.

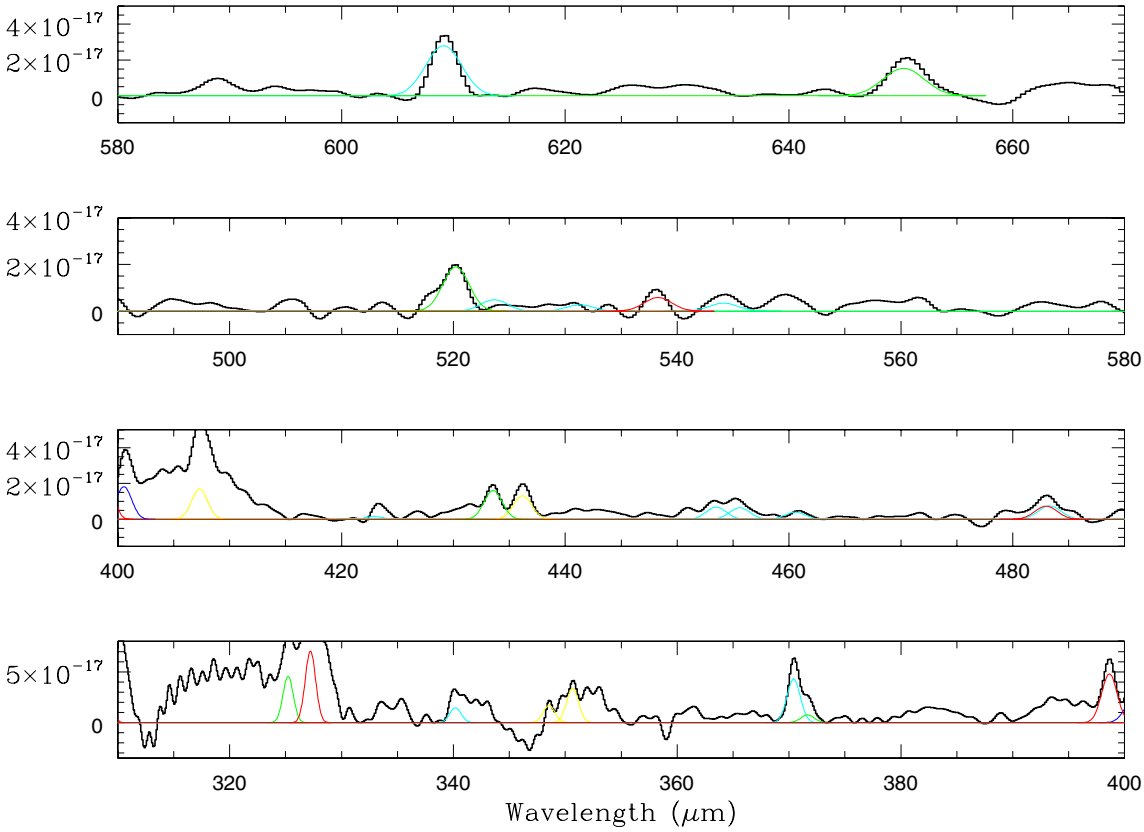

Fig. D.6. The continuum subtracted apodized SPIRE spectrum of OH 26.5+0.6,

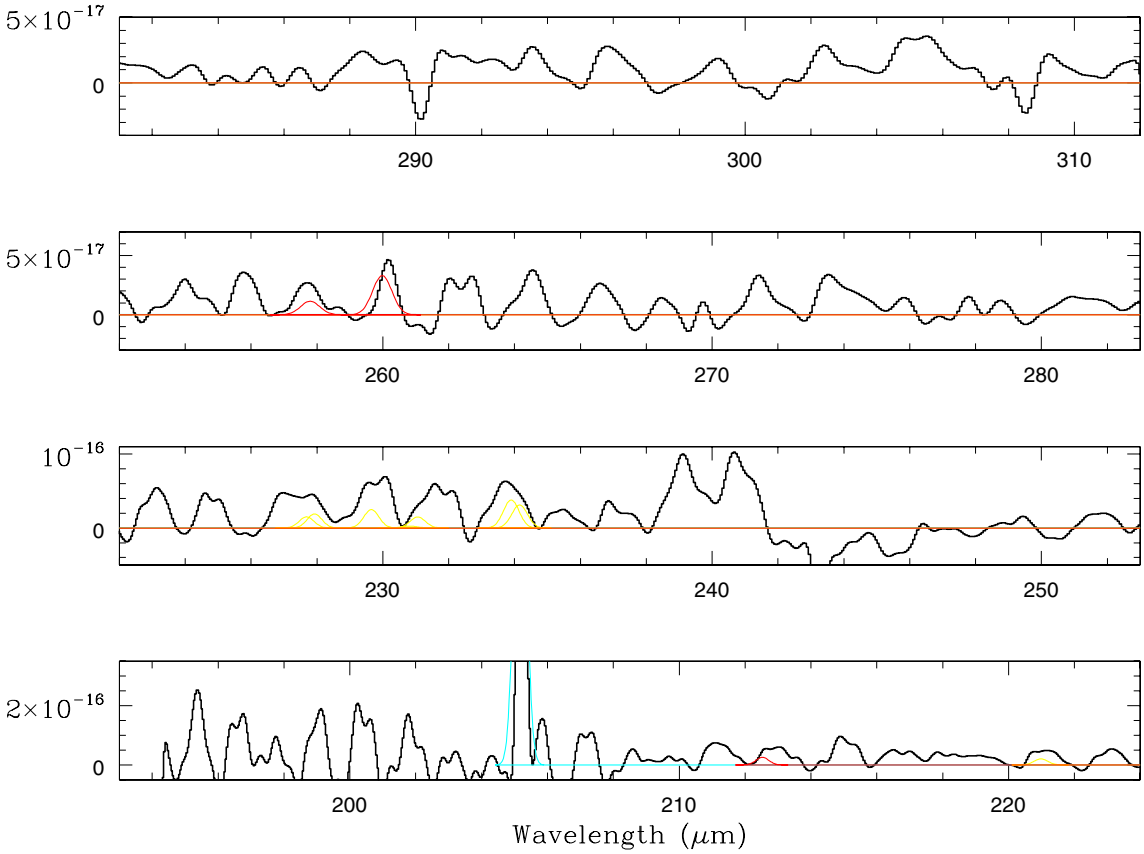

Fig. D.7. The continuum subtracted apodized SPIRE spectrum of OH 30.7+0.4.

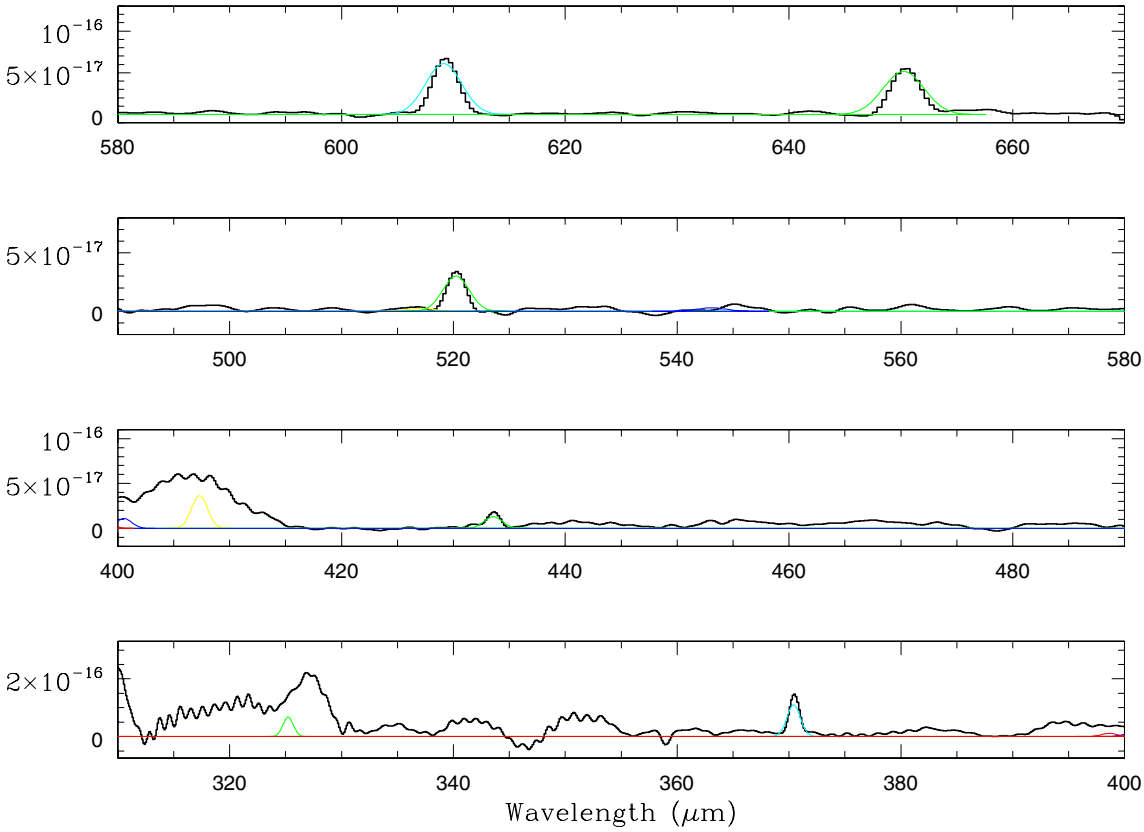

Fig. D.8. The continuum subtracted apodized SPIRE spectrum of OH 30.7+0.4.

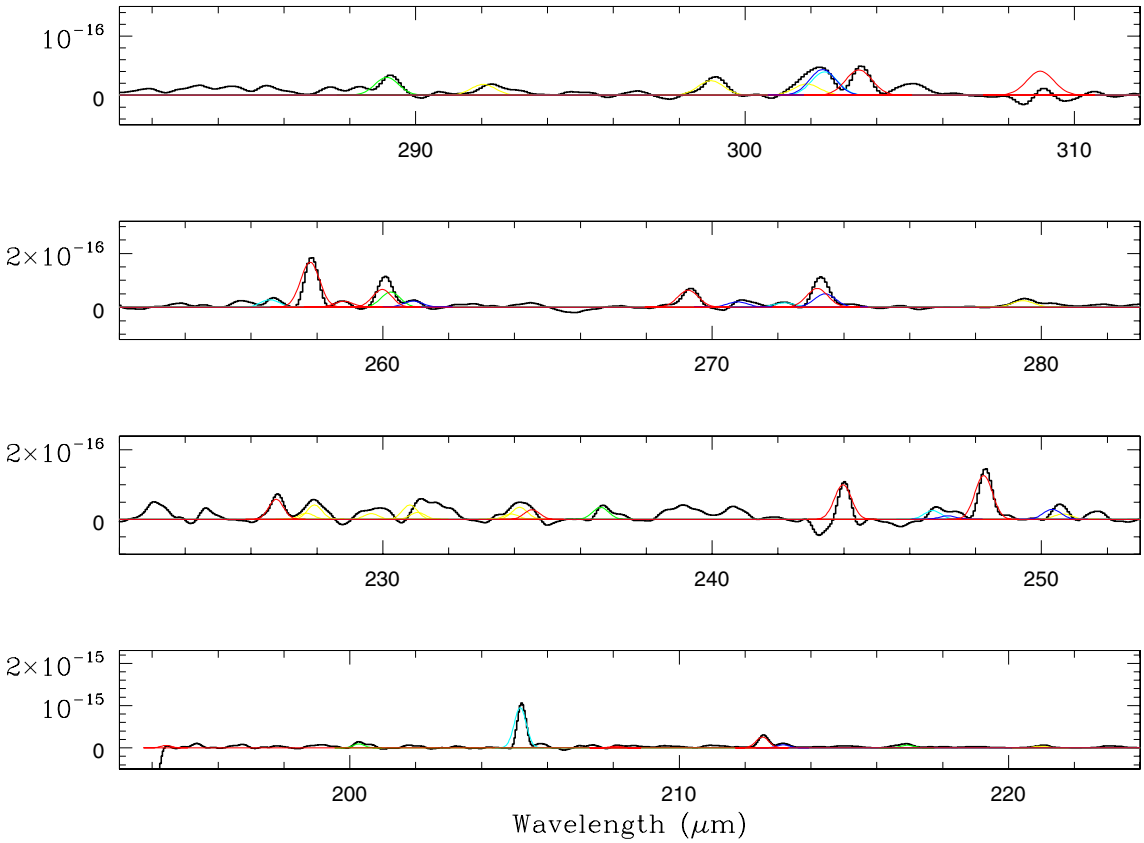

Fig. D.9. The continuum subtracted apodized SPIRE spectrum of OH 30.1-0.7.

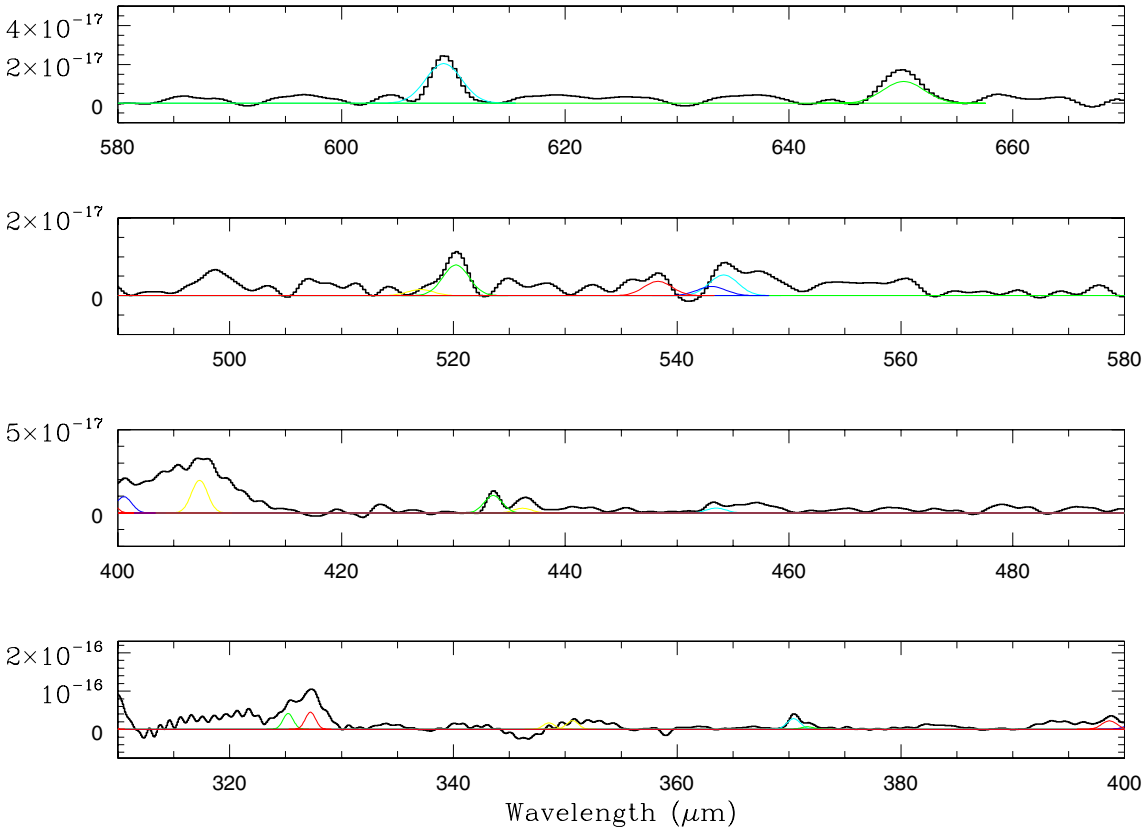

Fig. D.10. The continuum subtracted apodized SPIRE spectrum of OH 30.1-0.7.

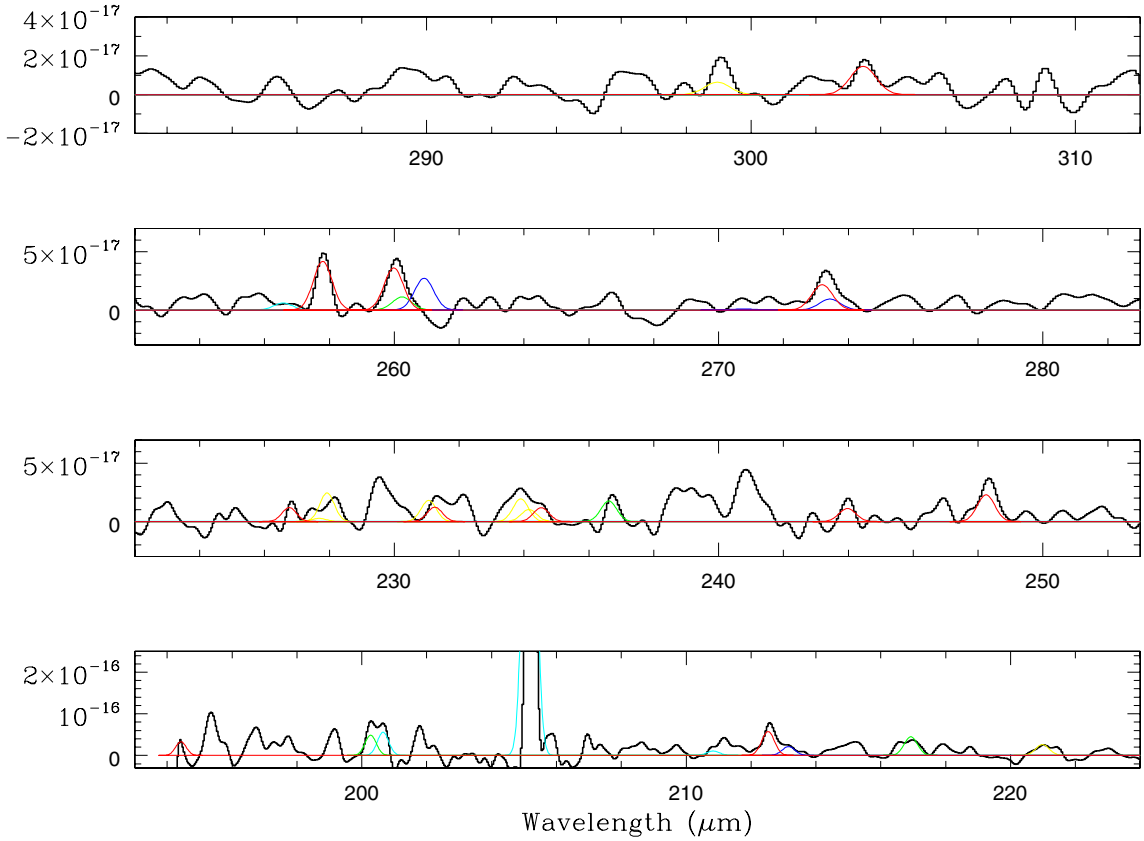

Fig. D.11. The continuum subtracted apodized SPIRE spectrum of OH 32.0-0.5.

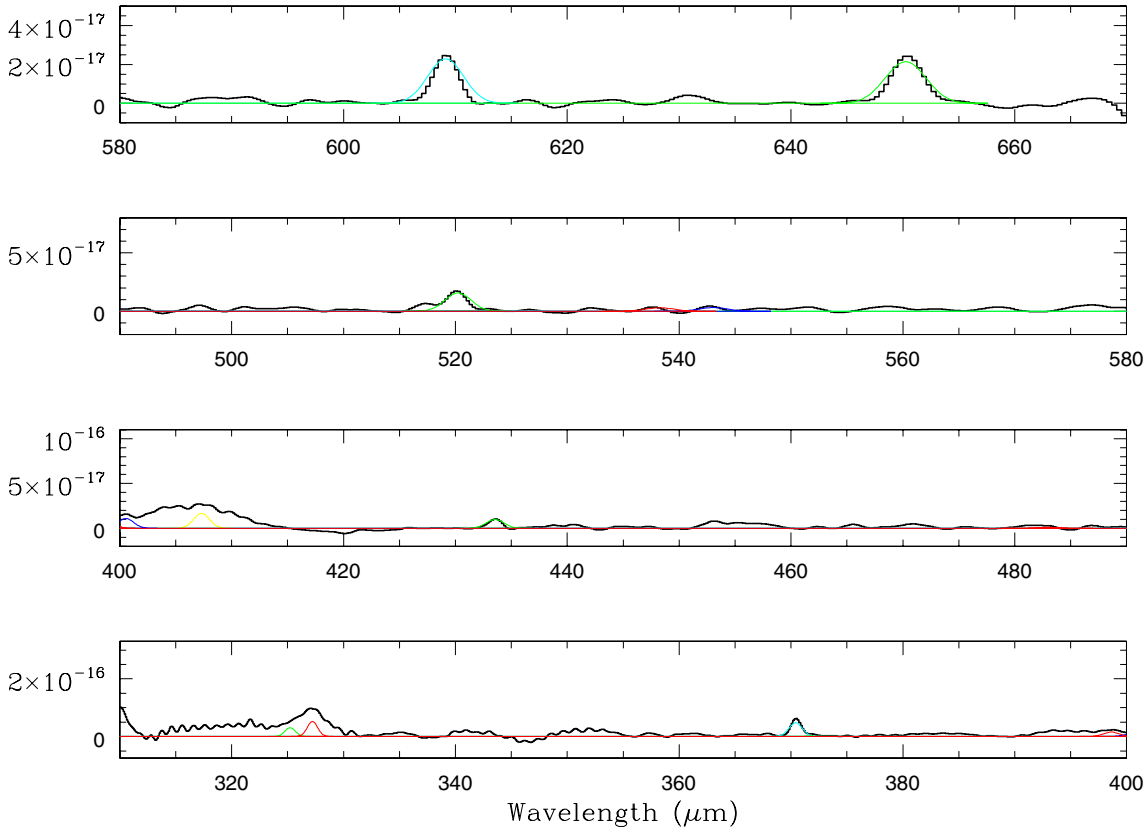

Fig. D.12. The continuum subtracted apodized SPIRE spectrum of OH 32.0-0.5.

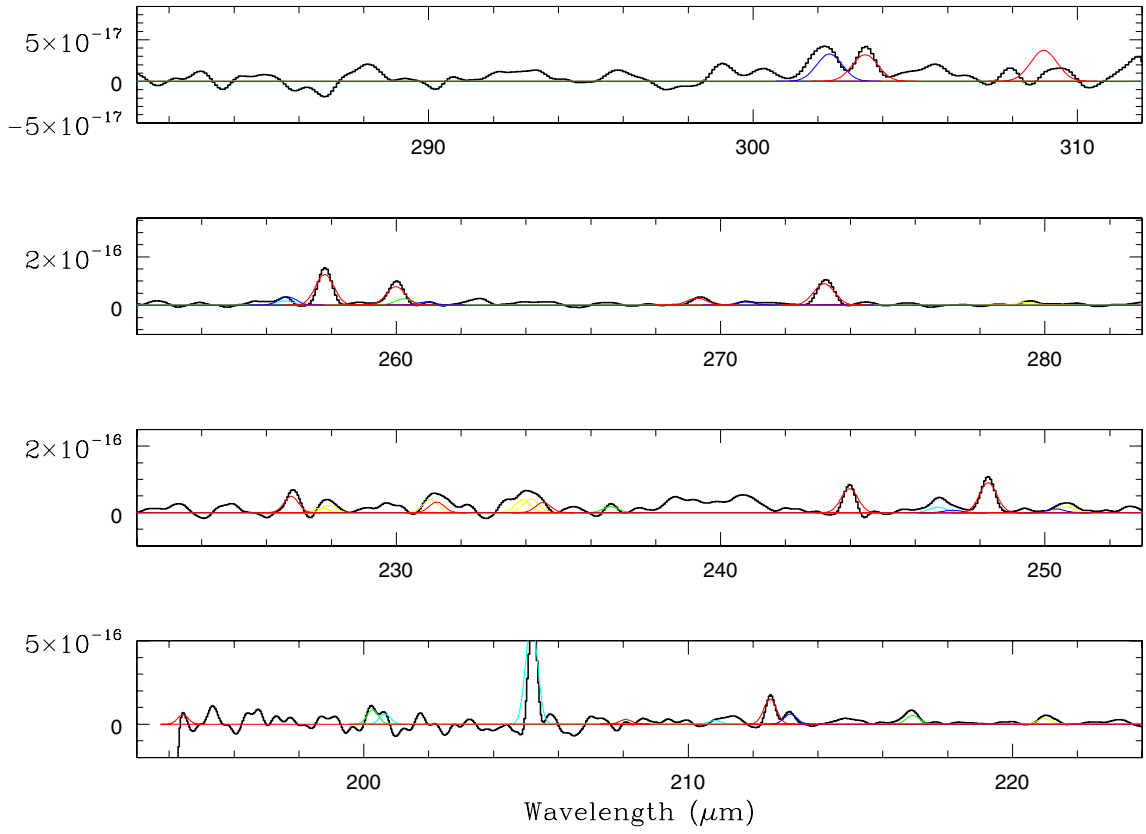

Fig. D.13. The continuum subtracted apodized SPIRE spectrum of OH 32.8-0.3.

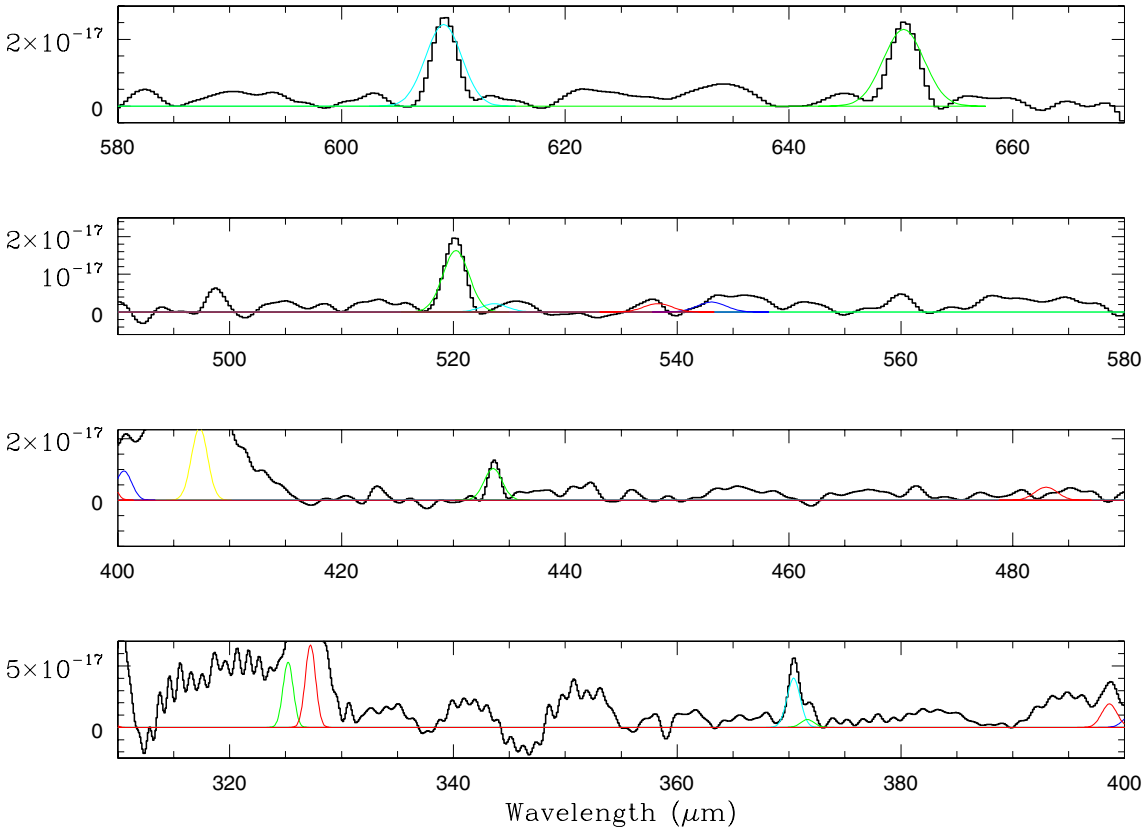

Fig. D.14. The continuum subtracted apodized SPIRE spectrum of OH 32.8-0.3.

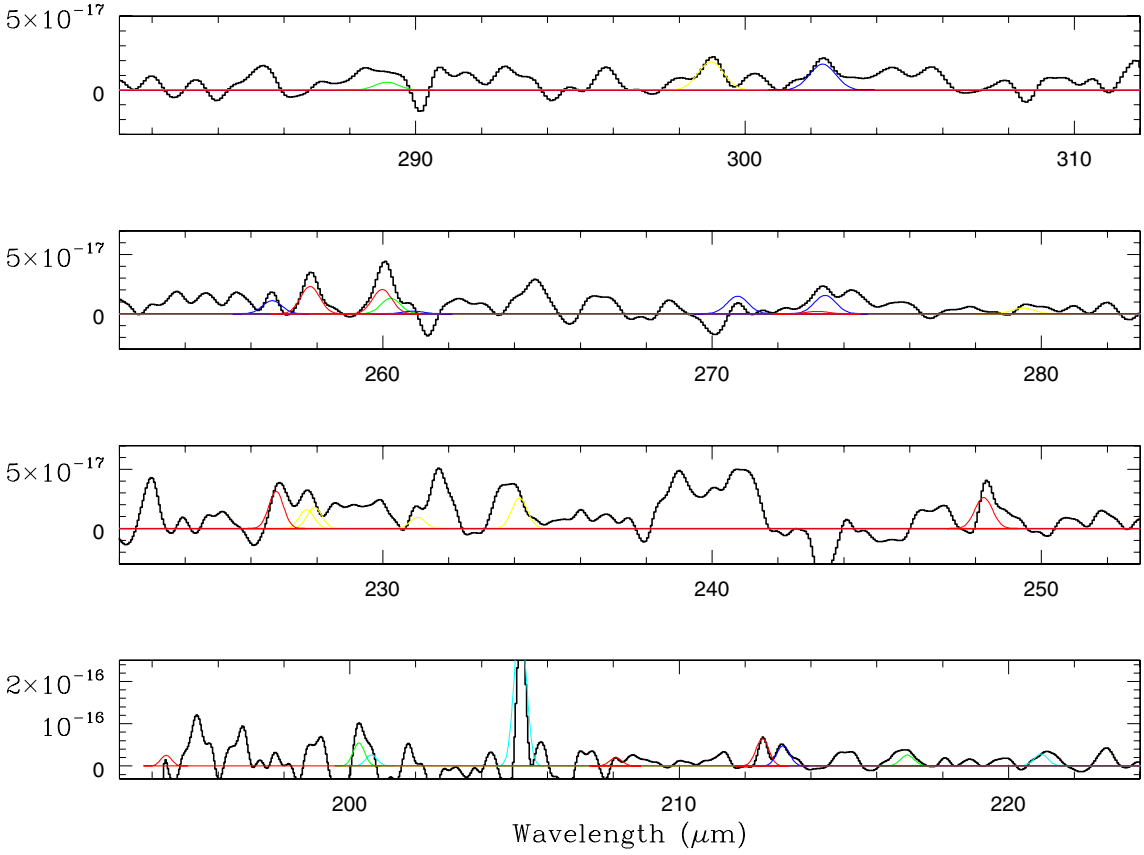

Fig. D.15. The continuum subtracted apodized SPIRE spectrum of OH 42.3-0.1.

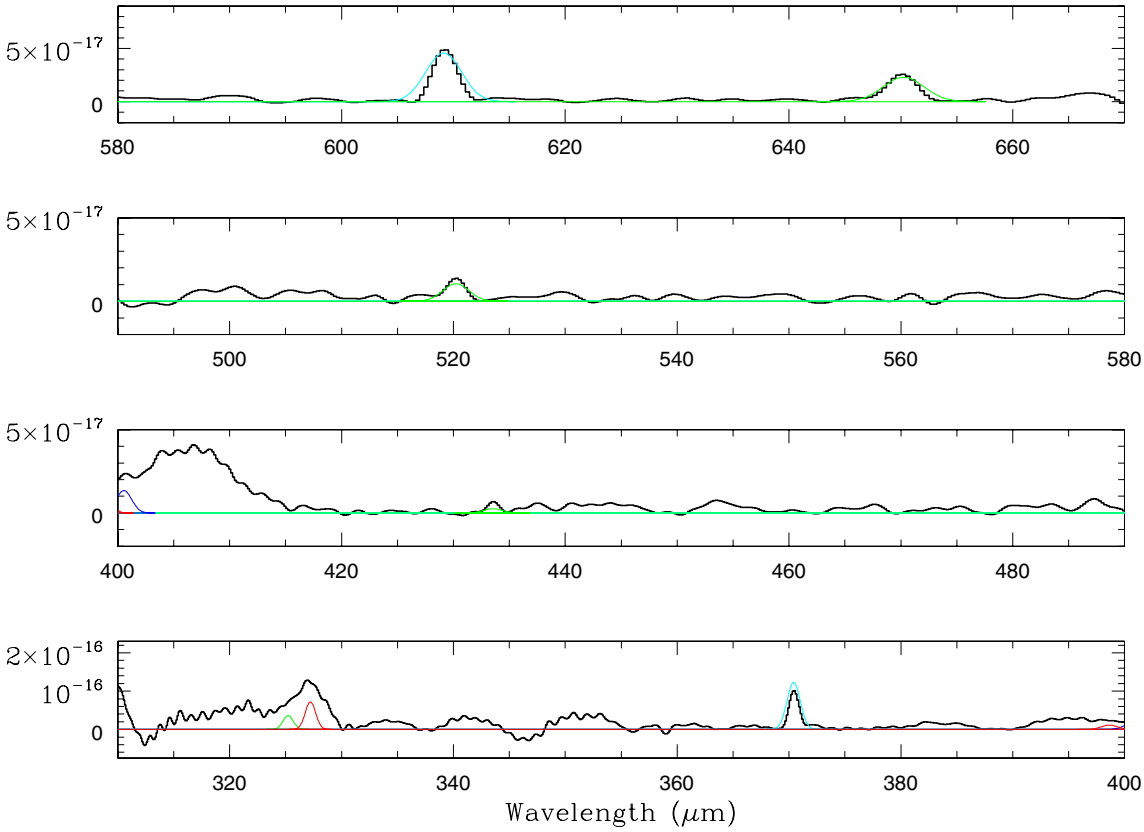

Fig. D.16. The continuum subtracted apodized SPIRE spectrum of OH 42.3-0.1.

Appendix E: PACS spectra

This section shows the continuum subtracted PACS spectra (in W $m^{-2}\mu m^{-1}$) of the stars in our sample (histogram) together with the Gaussian fits for H_2O (red), $H_2^{17}O$ (blue), and CO (green). Other molecules are shown in cyan. We note that no circumstellar emission lines are detected in the spectrum of OH 21.5+0.5. The PACS spectrum of OH 127.8+0.0 has already been publish by Lombaert et al. (2013) and is not presented here.

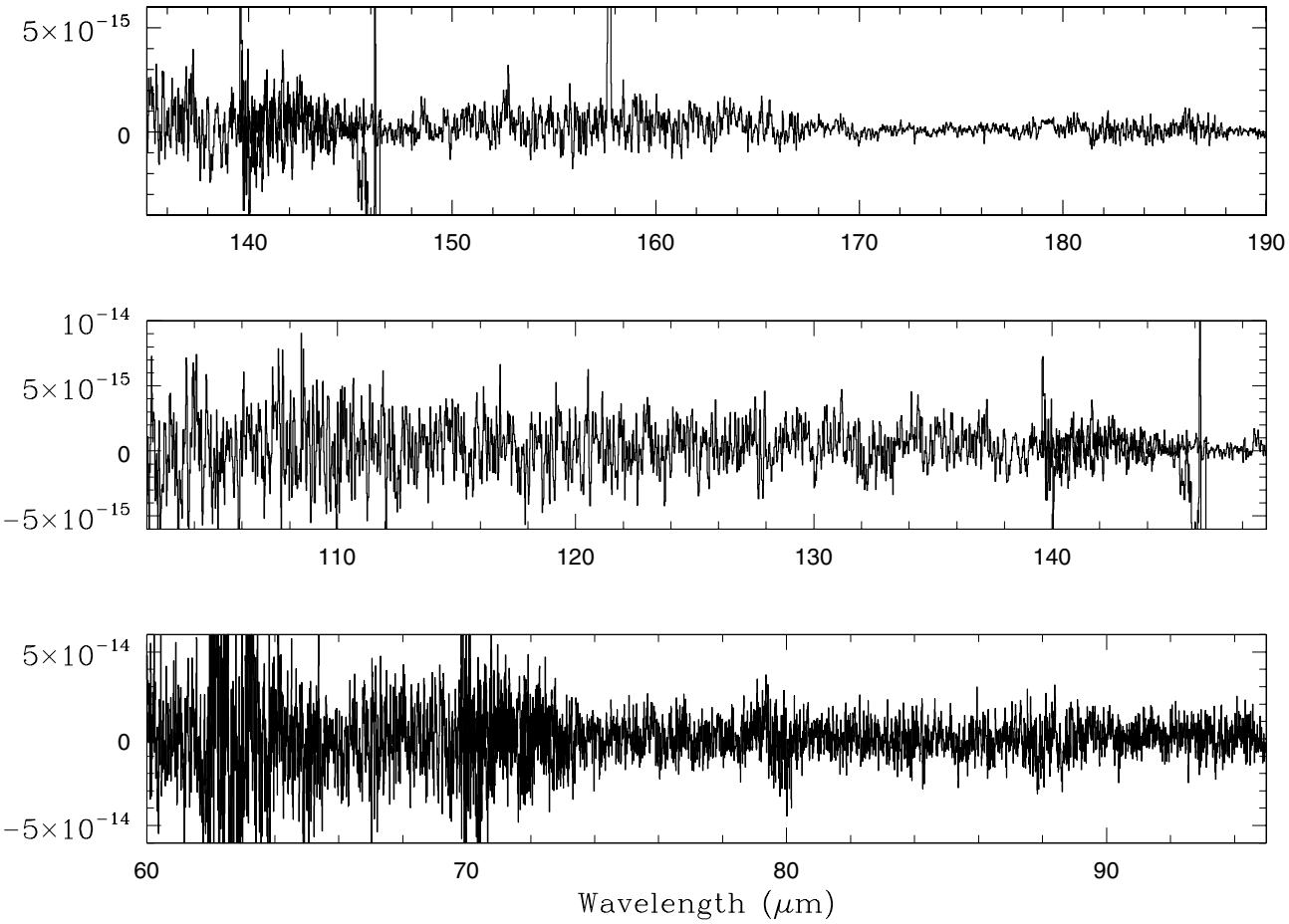

Fig. E.1. The continuum subtracted PACS spectrum of OH 21.5+0.5.

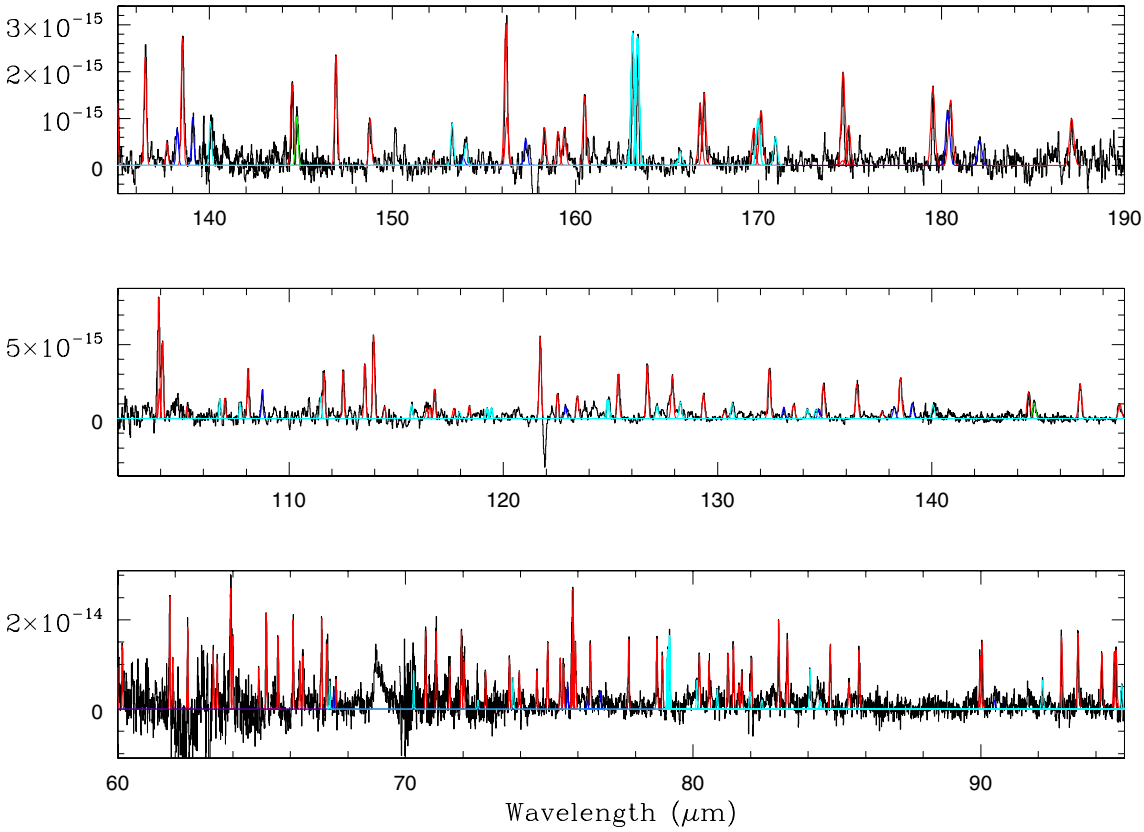

Fig. E.2. The continuum subtracted PACS spectrum of OH 26.5+0.6.

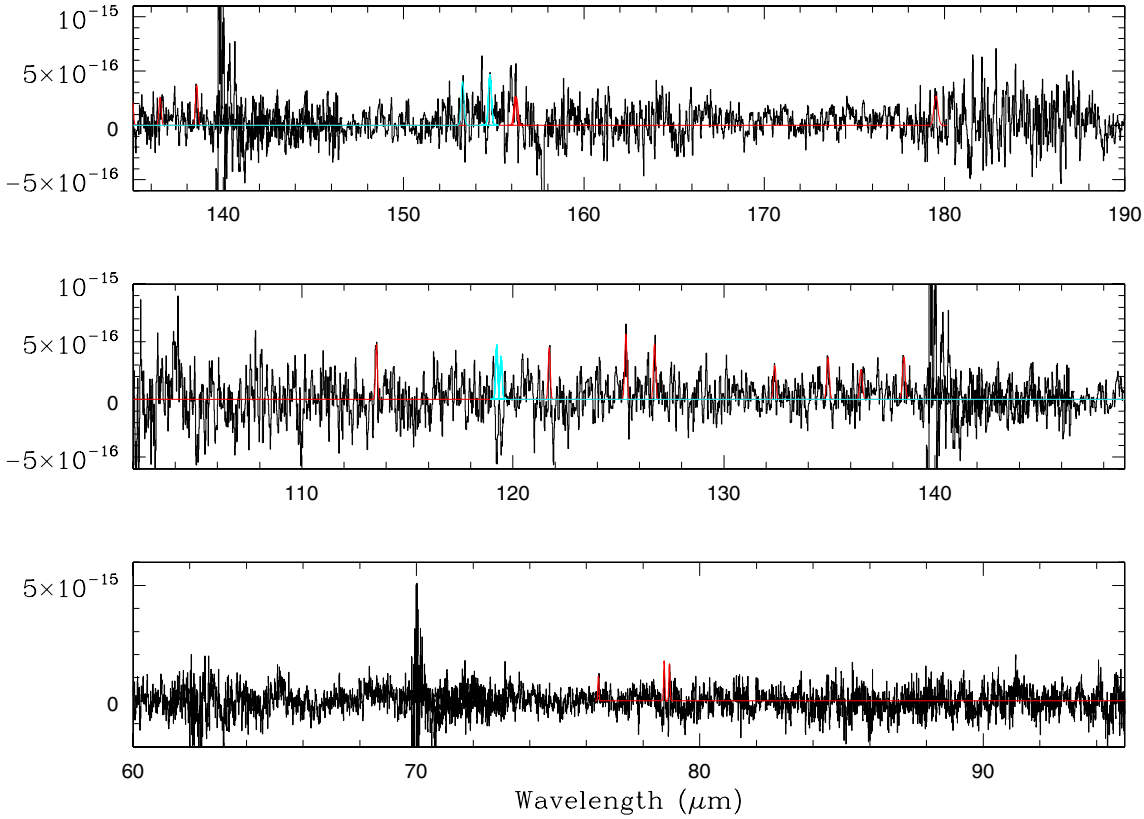

Fig. E.3. The continuum subtracted PACS spectrum of OH 30.7+0.4.

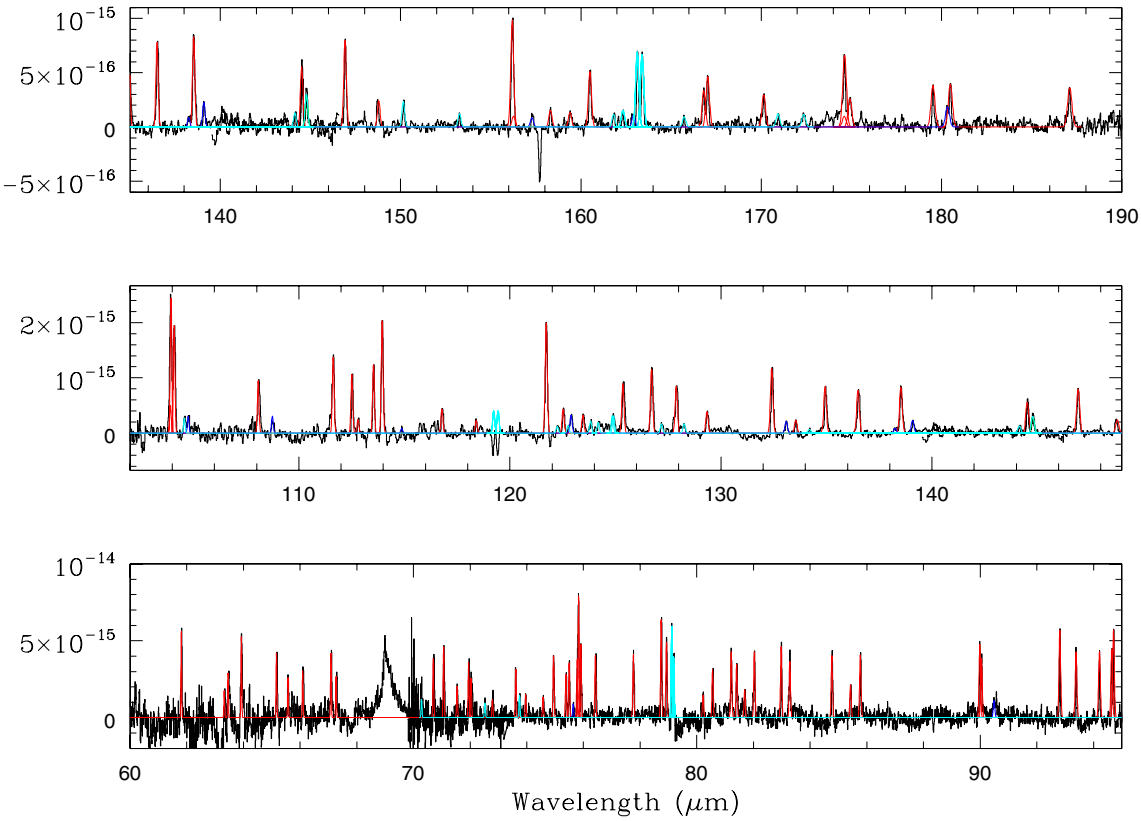

Fig. E.4. The continuum subtracted PACS spectrum of OH 30.1-0.7.

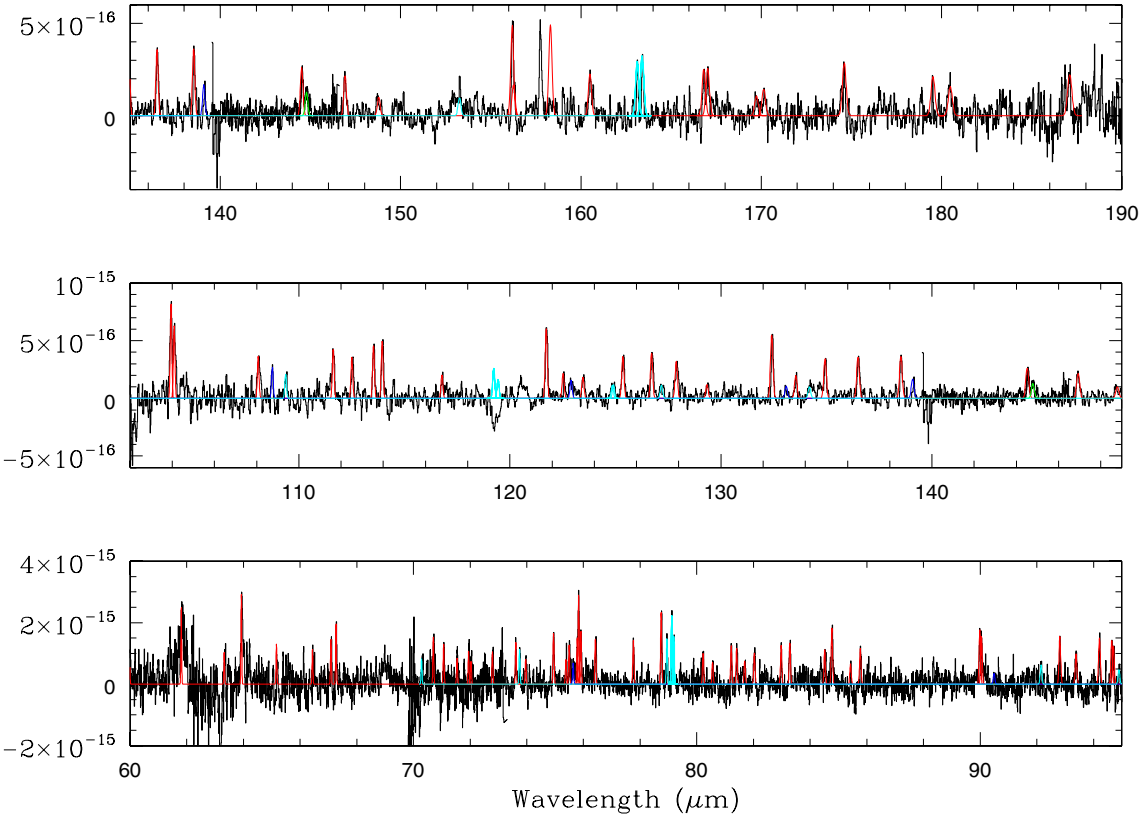

Fig. E.5. The continuum subtracted PACS spectrum of OH 32.0-0.5.

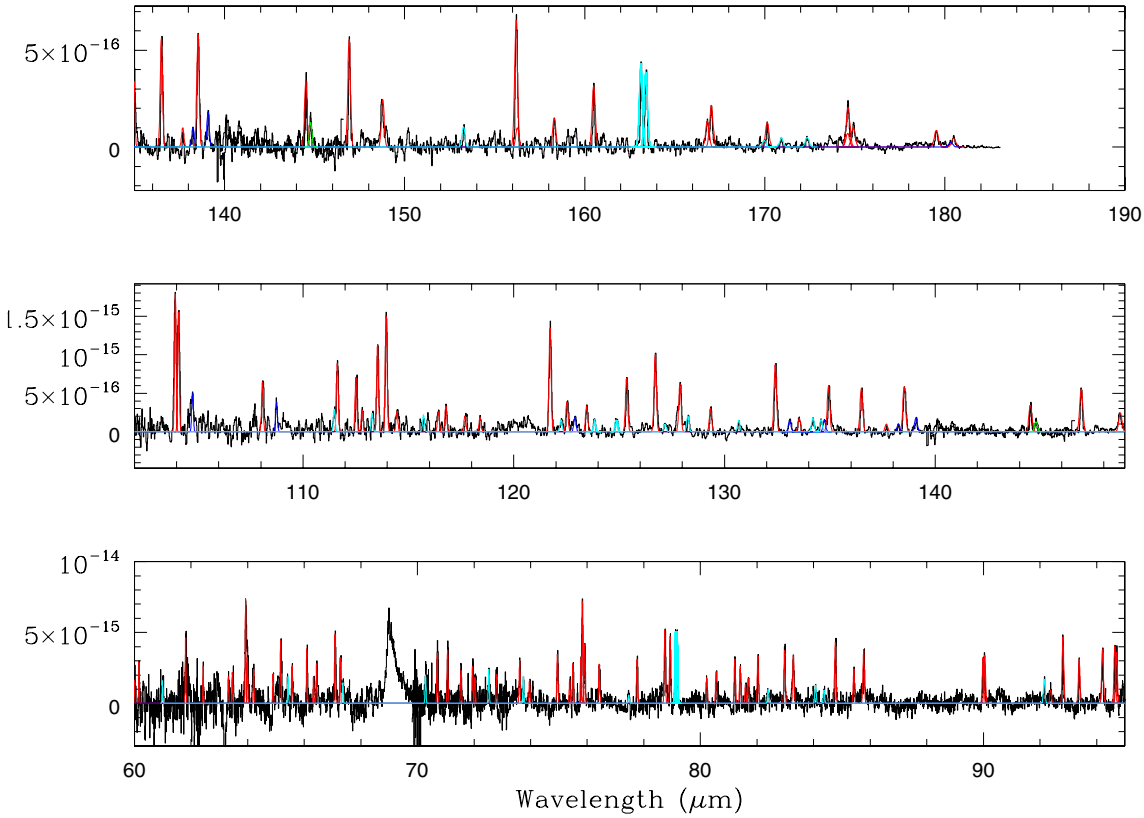

Fig. E.6. The continuum subtracted PACS spectrum of OH 32.8-0.3.

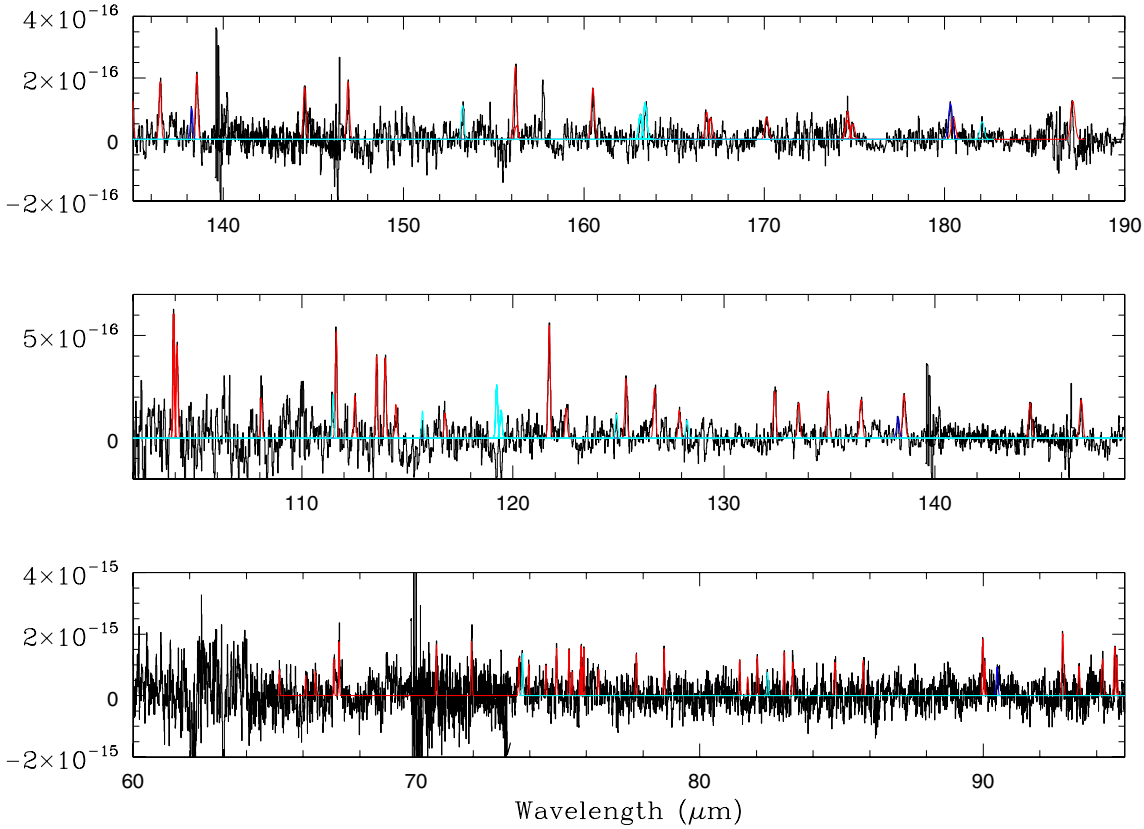

Fig. E.7. The continuum subtracted PACS spectrum of OH 42.3-0.1.